

**UC Davis**

**UC Davis Electronic Theses and Dissertations**

**Title**

Spectral Power Distribution Design using Quasi-Monochromatic LEDs and Cathodoluminescent Phosphor Lamps

**Permalink**

<https://escholarship.org/uc/item/6qs6t5sp>

**Author**

Lopez Osses, Claudio Salomon

**Publication Date**

2022

Peer reviewed|Thesis/dissertation

Spectral Power Distribution Design using  
Quasi- Monochromatic LEDs and Cathodoluminescent Phosphor Lamps

By

CLAUDIO LOPEZ OSSES  
DISSERTATION

Submitted in partial satisfaction of the requirements for the degree of

DOCTOR OF PHILOSOPHY  
in

Electrical and Computer Engineering

in the

OFFICE OF GRADUATE STUDIES

of the

UNIVERSITY OF CALIFORNIA

DAVIS

Approved:

---

Charles Hunt, Chair

---

Diego Yankelevich

---

Joshua Hihath

Committee in Charge

2022

## Acknowledgment

# Table of Contents

## Chapter 1

<b>1.1 Introduction</b> .....	<b>1</b>
<b>1.2 Background</b> .....	<b>2</b>
1.1.1 Light.....	2
1.1.2 Radiometry and Photometry .....	3
1.1.3 Color Vision .....	7
1.1.4 Colorimetry .....	9
1.1.4.1 Three-Color matching .....	9
1.1.4.2 Tristimulus Values.....	11
1.1.4.3 Chromaticity.....	13
1.1.4.4 Color Mixing .....	14
<b>1.3 Literature Review</b> .....	<b>16</b>
1.3.1 Light Sources Selection, Fabrication and Spectral Characterizations .....	16
1.3.1.1 Preserving Museum Artifacts.....	17
1.3.1.2 Plant Growth.....	18
1.3.2 Monochromatic Sources .....	19
1.3.2.1 Light Emitting Diode .....	19
1.3.2.2 Cathodoluminescence Phosphor Lamps.....	24
1.3.3 Genetic Algorithms .....	29

## Chapter 2: Experimental Design and Modeling

<b>2.1 SPD Characterization and Measurements of LEDs</b> .....	<b>32</b>
<b>2.2 SPD Characterization and Measurements for Cathodoluminescent Phosphor Lamps</b> .....	<b>35</b>
<b>2.3 Selection of the Desired SPDs</b> .....	<b>40</b>
2.3.1 First SPD Selected: Preserving Museum Artifacts.....	41
2.3.2 Second SPD Selected: Plant growth’s Mc-Cree.....	43
2.3.3 Third SPD Selected: Plant growth absorption.....	44
<b>2.4 Computational Model for the SPD</b> .....	<b>46</b>
2.4.1 Mathematical Model.....	46
2.4.2 Genetic Algorithms Model .....	48

## Chapter 3: Results and Discussion

<b>3.1 Simulation Results Using Real QMLS</b> .....	<b>56</b>
3.1.1 Simulation results for the Preserving Museum Artifacts.....	57

3.1.2 Simulation results for the Mc-Cree PAR Spectrum .....	58
3.1.3 Simulation results for the Photosynthesis-Action Spectrum .....	60
<b>3.2 Experimental Results</b> .....	<b>61</b>
3.2.1 Experimental results for the Preserving Museum Artifacts .....	62
3.2.2 Experimental results for the McCree PAR Spectrum .....	63
3.2.3 Experimental results for the Photosynthesis-Action Spectrum .....	65
<b>3.3 Experimental Result Using Ideal QMLSs</b> .....	<b>66</b>
3.3.1 Simulated results for the Preserving Museum Artifacts .....	67
3.3.2 Simulated result for the Mc-Cree PAR Spectrum.....	69
3.3.3 Simulated result for the Photosynthesis-Action Spectrum.....	71
Chapter 4: Conclusions and Future Work	
<b>4.1 Conclusion and Outlook</b> .....	<b>74</b>
<b>5 References</b> .....	<b>77</b>
Appendix.....	86

## List of figures

Figure 1.1 Relative spectral power distributions of CIE illuminants A, D50, D65, and F2.....	6
Figure 1.2 The spectral power distribution of Planckian radiators at temperature of 4000 K, 5000 K, 6000 K and 7000 K.....	7
Figure 1.3 Normalized responsivity spectra curves of human cone cells, S,M, and L types and Rods.....	8
Figure 1.4 The spectral luminous efficiency function for photopic and scotopic vision.....	9
Figure 1.5 The Color-Matching Experiment. R, G, and B are sources of red, green, and blue light, whose amounts can be adjusted; C is the light whose color is to be matched. The diffusers result in uniform fields for viewing by the observer.....	10
Figure 1.6 trichromatic matching functions obtained by Stiles .....	11
Figure 1.7 The CIE 2° XYZ CMFs transformed CIE (2006) LMS cone fundamentals.....	12
<i>Figure 1.8 The CIE 1931 (x, y) Chromaticity Diagram, the colored boundary line represents the coordinates of intense monochromatic light. White light is a line in the center used as a reference point. The equal-energy point is located at the center and has the coordinates (x, y) = (1/3, 1/3).....</i>	<i>14</i>
Figure 1.9 Red, blue, and green spectral primary colors. The dash line is the sum or superimpose of the three primary colors which represent the mixed color or final spectrum.....	15
Figure 1.10 The absorption spectrum indicates the wavelengths of light absorbed by each pigment (e.g. chlorophyll).....	19
Figure 1.11. Forward-biased LED p-n junction. When one electron and one hole recombine near the junction one photon of light may be emitted.....	21
Figure 1.12 LED Structure, the radiation pattern is determined packing by the combination of the die emission, the reflector cup and the shape and refractive index of the polymer lens. a) LED structure, b) LED Structure from datasheet Cree® XLamp® XP-C LEDs.....	22
Figure 1.13. The spectral power distribution of a phosphor-coated LED (darker blue line) and a three color LED with peak wavelengths at 473 nm, 544 nm, and 616 nm (lighter blue line).....	23
Figure 1.14 Relative flux vs junction temperature (If=350 mA), a) White , Blue and Green b) Amber red-Orange and Red. datasheet Cree® XLamp® XP-C LEDs.....	23
Figure 1.15: Schematic representation of energies of processes in cathodoluminescence A) back-scattered primary electrons, B) back-scattered primary electrons with some energy loss, C) low-velocity secondary electron emission, hv) luminescence emission. [33,34].....	25
Figure 1.16: FIG. I. Models of luminescent transitions. (a) Direct recombination of a free electron and a hole (band-to-band transition); (b) transition of a free electron to an acceptor level (c) recombination	

transition of a donor electron with a free hole (d) transition between a donor and an acceptor (e) transition within a localized luminescent center [34].....	26
Figure 1.17 Individual spectral power distribution of AlN:Eu <sup>2+</sup> , β-sialon:Eu <sup>2+</sup> , Ca-α-sialon:Eu <sup>2+</sup> and CaAlSiN <sub>3</sub> :Eu <sup>2+</sup> .....	27
Figure 1.18 Schematic of the Vu1 light bulb.....	28
Figure 1.19 Cross-sectional view of FEL schematic.....	29
Figure 1.20 Flow char of Genetics algorithms.....	31
Figure1. 21 Chromosomes: Each bit contain some aspects of the solution.....	31
Figure 1.22 The crossover representation with a crossover point right in the middle of the chromosome.....	32
Figure 1.23 Mutation of Offspring.....	32
Figure 2.1 XP-C LEDs, all measurements are ±13mm unless otherwise indicated, a) Image of the LED, b) top and side view sizes, c) PCB solder pad, d) Bottom and alternate bottom view.....	35
Figure 2.2 The SPDs of the four LEDs collected by using ocean optics.....	36
Figure 2.3 Current versus Luminous Flux of the four LEDs.....	36
Figure 2.4 Layout of the testing system.....	38
Figure 2.5 Picture of the vacuum system built in the vacuum microelectronic laboratory.....	38
Figure 2.6 Schematic diagram for the electron gun.....	40
Figure 2.7 3D figure for the cathode.....	40
Figure 2.8 Schematic of phosphor screen sample.....	41
Figure 2.9 SPD of Red cathodoluminescent phosphor.....	42
Figure 2.10 SPD of blue cathodoluminescent phosphor.....	43
Figure 2.11 SPD of green cathodoluminescent phosphor.....	44
Figure 2.12 Mark 3 SPD target.....	46
Figure 2.13 The Action spectrum, absorptance and quantum yield of photosynthesis in crops plants.....	48
Figure 2.14 The upper subplot shows the absorption spectra of chlorophylls a and b, and carotenoid pigments. The lower subplot shows the photosynthetic action spectrum.....	49
Figure 2.15. Schematic examples of some idealized phosphor screens: (a) superimposed-layer screen; (b) mixed-phosphor screen; (c) onionskin phosphor screen.....	47
Figure 2.16 Four genes at 100%, 75%, 50% and 25% of their maximum intensities normalized.....	51
Figure 2.17 Chromosomes: Each gene modifies the intensity of a single QMLS.....	52

Figure 2.18 Four chromosomes each composed by four SPDs.....	53
Figure 2.19 Matrix of four possible solutions with four QMLSs.....	55
Figure 2.20: Ranking for each chromosome after the fitness evaluation.....	56
Figure 2.21: Matrix obtained after sorting the initial population by the ranking.....	56
Figure 2.22: Description of the New matrix after the selection process.....	57
Figure 2.23 Matrix after the selection process.....	57
Figure 2.24 Matrix after the crossover process.....	58
Figure 2.25 Matrix after mutation.....	58
Figure 3.1: SPD simulation results for fitting the preserving museum artifact’s SPD.....	61
Figure 3.2: SPD simulation results for fitting the plant growth’s McCree SPD.....	62
Figure 3.3: SPD simulation results for fitting the photosynthesis active Spectrum’s SPD.....	63
Figure 3.4: Experimental response for the Preserving Museum artifact’s SPD.....	65
Figure 3.5: Experimental responses of the Plant Growth’s MC Cree’s SPD.....	66
Figure 3.6: Experimental Fits answer for the photosynthesis active spectrum’s SPD.....	68
Figure 3.7: SPD light results using a different quantity of ideal QMLSs to fit in a preserving museum artifacts SPD .....	70
Figure 3.9: SPD light results using a different quantity of ideal QMLSs to fit in a Plant Growth’s McCree’s SPD.....	72
Figure 3.10: SPD results using a different quantity of ideal QMLSs to fit a photosynthesis active spectrum’s SPD using ideal QMLSs.....	74



## List of Tables

Table 2.1 Wavelength peaks and flux of LEDs taken by the datasheet.....	35
Table 2.2 Characteristic of Mark 3 SPD. ....	46
Table 2.3 Perceptual attributes of color result from Mark 3 SPD.....	47
Table 3.1: Individual intensity results for the QMLS's to fit the preserving museum artifact's SPD.....	60
Table 3.2: Individual intensity results for the QMLS's to fit the Plant growth's McCree's SPD.....	61
Table 3.3: Individual intensity results for the QMLS's to fit the photosynthesis active spectrum's SPD....	63
Table 3.4. Excitation values and the final SPD response using the BGAR lamp.....	65
Table 3.5: Excitation values and the final SPD response using the BGR lamp.....	65
Table 3.6: Excitation values and the final SPD response using the BAR lamp.....	65
Table 3.7. Excitation values and the final SPD response using the BGAR lamp.....	66
Table 3.8: Excitation values and the final SPD response using the BGR lamp.....	66
Table 3.9: Excitation values and the final SPD response using the BAR lamp.....	66
Table 3.10: Excitation values and the final SPD response using the BGAR lamp.....	67
Table 3.11: Excitation values and the final SPD response using the BGR lamp.....	67
Table 3.12: Excitation values and the final SPD response using the BAR lamp.....	67
Table 3.13: Peak wavelength bounds used in the GA model for the preserving museum artifacts' SPD...69	
Table 3.14 Simulated parameters results for the preserving museum artifacts by using ideals QMLSs....	70
Table 3.15: Peak wavelength bounds used in the GA model for the Plant Growth's McCree's SPD.....	71
Table 3.16: Simulated parameters results for the Plant Growth's McCree's SPD using ideal QMLSs.....	71
Table 3.17: Peak wavelength bounds used in the GA model for the photosynthesis active spectrum's SPD.....	73
Table 3.18: Simulated parameters results for the photosynthesis active spectrum's SPD using ideal QMLSs.....	73

## Abstract

This dissertation contributes to the investigations of the organic and inorganic materials' reactions to the light sources, describing the artificial light sources and some of the problems due to the absorption of this light in organic materials. Its main focus is on using the available technologies to obtain a spectrum that accomplishes an ideal Spectral Power Distribution (SPD) for special applications such as plant growth and art exhibits.

The developed model uses a genetic algorithm approach to optimize the parameters that produce the desired SPD by combining artificial light sources. The model is versatile and can be used for different variables, such as the light intensities or even the spectrum of single light sources.

The work considered emulating three different desired SPDs identified to contribute in the agricultural plant and in the art venues where preserving museum artifacts is crucial. The artificial light sources implemented were based on Light Emitting Diodes (LEDs) and Cathodoluminescence Phosphor Lamp (CL) and grouped into two, three, or four quasi-monochromatic light sources for the evaluation. This study implemented a vacuum testing system to obtain the SPD data for different CL phosphor materials and mixtures.

The genetic algorithm model, the SPD pre-processing, and analysis was carried out using MATLAB. The model used the R-Square function to evaluate how much the obtained spectrum fits the desired spectrum. The simulation results of the genetics algorithms model were implemented using LEDs

The GA method was applied to different groups of Quasi-Monochromatic Light sources (QMLSs) and LEDs, showing promising results with the optimized parameters.

# Chapter 1

## 1.1 Introduction

Energy efficiency is one of the main factors when selecting a light source, and nowadays, a variety of light sources can fulfill this requirement <sup>(1)</sup>. However, some researchers from different areas of knowledge have demonstrated that besides the energy efficiency, the spectral power distribution (SPD) plays a significant role in defining the perceived colors on an object and the human observer's response. Additionally, the investigations about how radiation affects organic and inorganic materials have placed the light's SPD as one of the main concerns for the light source selection. In the preserving museum artifacts field, the artifacts' damage is caused by its exposure to some SPD wavelength ranges. Thus, the damage can be reduced by SPD manipulation that decreases the intensity in those critical ranges <sup>(2,3,4,5)</sup>. In agriculture, the light's SPD influences the plants' growth stages, and its manipulation can enhance photosynthesis <sup>(6,7,8)</sup>. There is also research about the photochemical damage and intoxication of the retina that can occur because of the exposure to artificial light, especially from the radiation's impact from the blue-violet part of the spectrum. On the other side, blue-light emissions are essential not only for color recognition but also for non-visual processes like melatonin secretion regulation, pupil's reflex to light, the cognitive abilities, mood, motor system, memory, and body temperature <sup>(9,10)</sup>.

A technique commonly used to design light sources that produce the desired SPD is the color mixing that combines different color light sources. This procedure is expensive because of the increment in power sources, but also exhibits many advantages, such as the easy modifying of the SPD by changing the excitation variables in the single light sources. This versatility helps when single light source proportions require adjustment at different intensity rates. This technique also has the advantage of replacing a single light source. The main disadvantages of this approach is related to the selecting of the color sources and the intensities, but this work presents a novel method to solve this problem.

Light Emitting Diodes (LED) and cathodoluminescent (CL) phosphor lamps are energy-efficient and quasi-monochromatic light sources that can be combined into one new SPD. Thus, the output light can be deducted using radiometric tools such as additive color mixing<sup>(11,12)</sup>. The selection of the quasi-monochromatic light source (QMLS) peak and the intensities to mimic a required SPD is an optimization problem<sup>(5)</sup> that can be solved using Genetic Algorithms (GAs).

This research, created a novel MATLAB App to obtain adequate variables to build a lamp with a specific SPD by combining various quasi-monochromatic light sources. This App predicts the individual LEDs and CL Phosphor lamps' excitation parameters to obtain an SPD profile as close to the desired SPD as possible.

## 1.2 Background

This section presents a series of definitions and concepts essential to understanding the light sources, Their content, and characteristics such as light, radiometry, photometry, and color space.

### 1.2.1 Light

It is electromagnetic waves that propagate radiant energy that can be described by its frequency  $f$  or wavelength  $\lambda$ . The wavelength of light that make vision possible to the human eye is confined to a very narrow range limited by a short-wavelength edge between 360 and 450 nm and a long-wavelength edge between 650 and 730 nm. The amount of energy in each photon or carried by a wave is calculated by the equation 1 <sup>(11,12)</sup>.

$$E = \frac{2.0 \cdot 10^{-16}}{\lambda} \quad \text{equation 1}$$

Where E is in SI units of Joules (J) and the wavelength is in nanometers (nm).

### 1.2.2 Radiometry and photometry

Radiometry is the system used to describe and measure the energy content and the propagation of electromagnetic radiation. The results of a radiometric measurement are usually obtained in units of power in Watts, photon flux (photons per second) or in units of energy (Joules) or dose (Photons) <sup>(12,13)</sup>.

*Radiant Energy [Q with units of Joule]:* It is the energy in the form of electromagnetic radiation emitted, transferred, or received <sup>(13)</sup>.

*Radiant Power* [ $\Phi$  with units of Watt]: Also called radiant flux is the power emitted, transferred, or received in the form of electromagnetic radiation <sup>(12,13)</sup>.

$$\Phi = \frac{dQ}{dt} \quad \text{equation 2}$$

The concepts of *irradiance*, *intensity*, and *radiance* involve the density of the radiant power over the area, solid angle, and area times solid angle respectively <sup>(12,13)</sup>.

In photometry, the same radiation transfer concepts as those for radiometry are used. However, they apply to a restricted portion of the electromagnetic spectrum due to the spectral responsivity of the human eye, which is related to radiometric quantities via the spectral efficiency functions defined for the photopic and scotopic CIE Standard Observer <sup>(12,13)</sup>.

*Luminous flux* is the spectral radiant flux weighted by the eye response function and its unit is the lumen. The equation for the luminous flux is shown in the equation 3 <sup>(12,13)</sup>.

$$\Phi_v = k_m \int_{380}^{830} \Phi_\lambda V(\lambda) d\lambda \quad \text{equation 3}$$

Where  $V(\lambda)$  is called the Luminosity Function, a unitless quantity. It represents the brightness based on a standardized model of the sensitivity of the human eye.

*Luminous Intensity* is the luminous flux per solid angle and its unit is the candela <sup>(12,13)</sup>.

$$I_v = \frac{dQ_v}{d\Omega} = \frac{d\left[k_m \int_{380}^{830} \Phi_\lambda V(\lambda) d\lambda\right]}{d\Omega} \quad \text{equation 4}$$

The candela (*cd*) is defined by international agreement as the luminous intensity in a given direction of a source that emits monochromatic radiation of 555.016 nm with a spectral luminous efficacy of 683 lm/W.

*Luminance* is the luminous flux per unit area per unit solid angle, its unit is the candelas/m<sup>2</sup>(13).

$$L_v = \frac{d\Phi}{\cos\theta_s dA_s d\Omega} = \frac{d\left[k_m \int_{380}^{830} \Phi_\lambda V(\lambda) d\lambda\right]}{\cos\theta_s dA_s d\Omega} \quad \text{equation 5}$$

*Illuminance* is the luminous flux per unit area and the unit is lux (lx) or lumens/m<sup>2</sup> (12,13).

$$E_v = \frac{\Phi}{A} = \frac{I\Omega}{r^2\Omega} = \frac{I}{r^2} = \frac{d\Phi}{\cos\theta_d dA_d} = \frac{d\left[k_m \int_{380}^{830} \Phi_\lambda V(\lambda) d\lambda\right]}{\cos\theta_d dA_d} \quad \text{equation 6}$$

Where r is the distance between the point and the surface.

*Spectral power distribution* (SPD) is the power emitted by a light source per unit wavelength. The SPD defines the perceived colors on an object depending on the illuminating light source, the reflection or transmission of light by the object, and the response of the human observer (12,13) which has the unit of lumens. It can be also referred to as the relative spectral distribution  $S(\lambda)$

$$S(\lambda) = \frac{X_\lambda(\lambda)}{R} \quad \text{equation 7}$$

Where  $X_\lambda(\lambda)$  is the radiant flux per wavelength, and R is “a fixed reference value which can be an average value, a maximum value or an arbitrarily chosen value of this distribution” (CIE, 2011) (12).

*Illuminants*

Standard illuminants are mathematical constructs that the Commission Internationale de L'Eclairage (CIE) established and published to provide a basis for comparing object color

appearances under different light sources. The method of comparing full-spectrum light sources is often referred to as mimicking daylight or blackbody radiation. The light from the sun has to pass through both its own atmosphere and that of the earth. There are only two sun's atmosphere absorptions most significant, and they are in the form of very narrow absorption lines. First, light is lost at the short-wavelength end of the spectrum due to the scattering of blue and ultraviolet radiation back into space. Second, light is absorbed by the molecules of various gases, particularly water vapor and ozone. The most common daylight standard illuminants are the CIE illuminant D50, and D65, with correlated color temperatures (CCT) of about 5000 K, 6500 K, respectively. The illuminant A represents the incandescent lamp at a temperature of 2856 K. The illuminant F2 described a fluorescent light source with cool-white light with CCT of 4230 K. Their SPDs are shown in Figure 1.1(13,14).

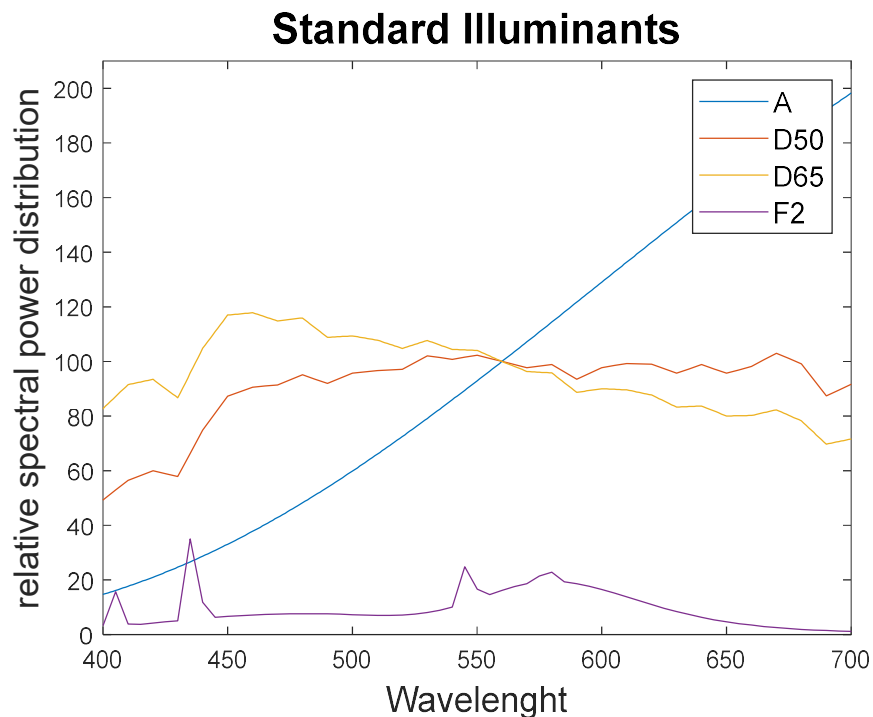




Fig. 1.1 Relative spectral power distributions of CIE illuminants A, D50, D65, and F2 (each normalized to the same relative power at 560 nm).

*Black body radiator* Another standard for characterizing the light sources is the color temperature. This classification is based on a blackbody radiator's physical concept, which is an ideal object that perfectly absorbs all the radiation incident on its surface and does not transmit or reflect any of the incident radiation. The blackbody or Planckian radiator is a thermal radiation source with a predictable absolute radiance output. According to Planck's law, the blackbody radiation is given by the equation 8.

$$2 M_e = \frac{2\pi hc^2}{n^2 \lambda^5} [e^{(hc/n\lambda k)} - 1]^{-1} \quad \text{equation 8}$$

Here the  $h$  is Planck's constant,  $c$  is the speed of light in the vacuum,  $k$  is Boltzmann's constant,  $\lambda$  is the wavelength, and  $n$  is the index of refraction of the medium <sup>(11,12,13,14)</sup>. Figure 1.2 shows the curves in the visible range obtained by the equation 8 using different temperatures.

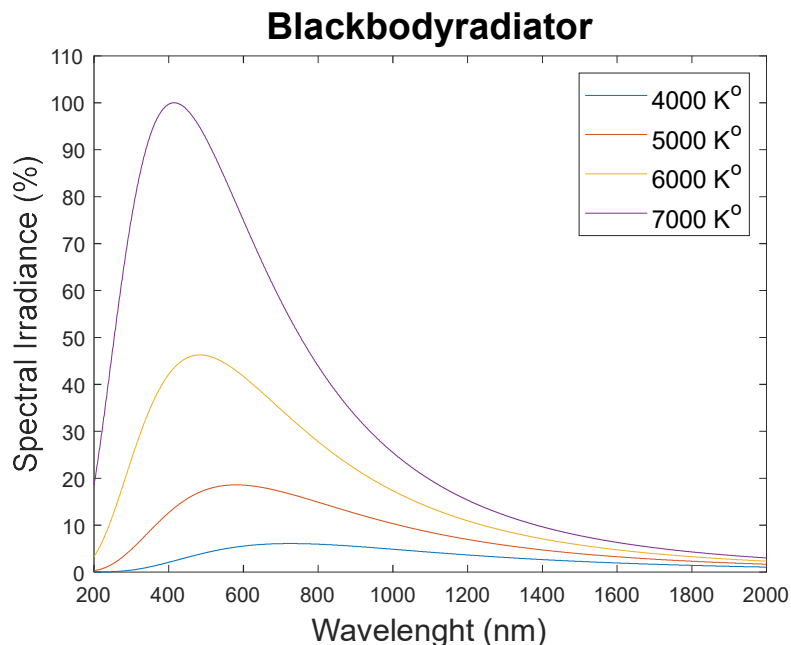


Fig. 1.2 The spectral power distribution of Planckian radiators at the temperatures of 4000 K, 5000 K, 6000 K and 7000 K.

### 1.2.3 Color vision

Our eyes have light-sensitive cell photoreceptors called rods and cones. The cones are categorized into three defined by the wavelength range that they can sense; the L cones are sensitive to the long optical wavelengths, whereas the M cones are more sensitive than the medium optical wavelengths, and the S cones sense the short optical wavelengths. All colors are defined by the degree of response of these photoreceptors. The rod cells are more sensitive than the cone cells and are responsible for the night vision. However, the rods have a much smaller role in the color vision. Figure 1.3 shows the normalized curves of sensitivity by the L, M, and S cones; and the rods.

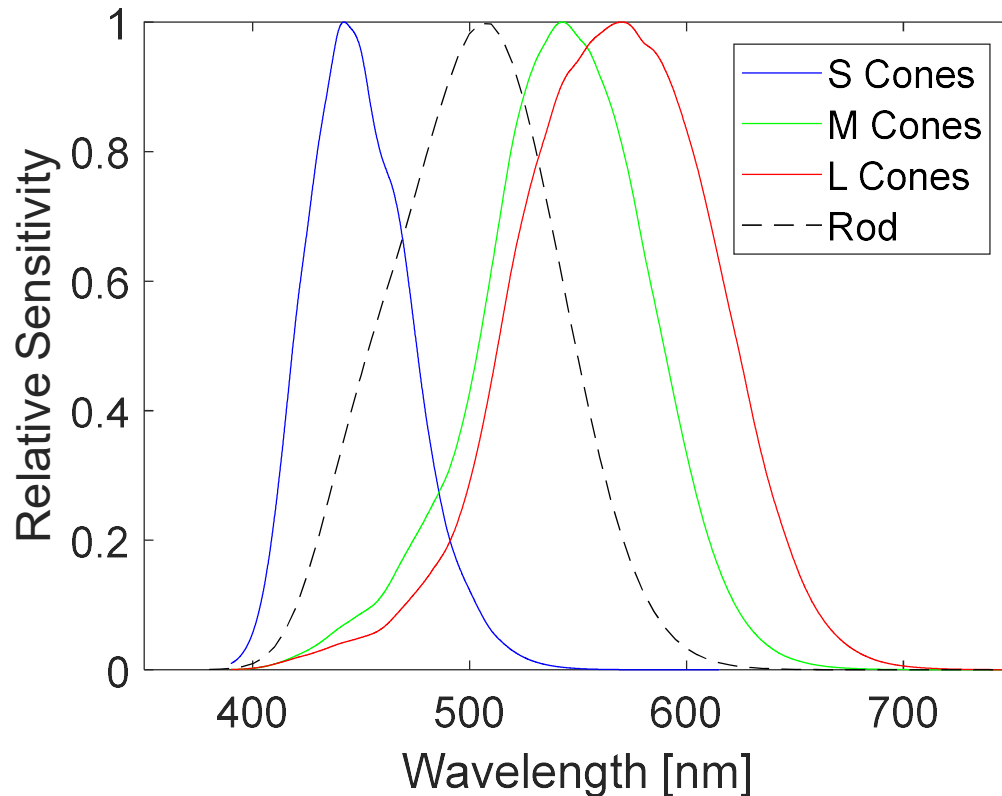
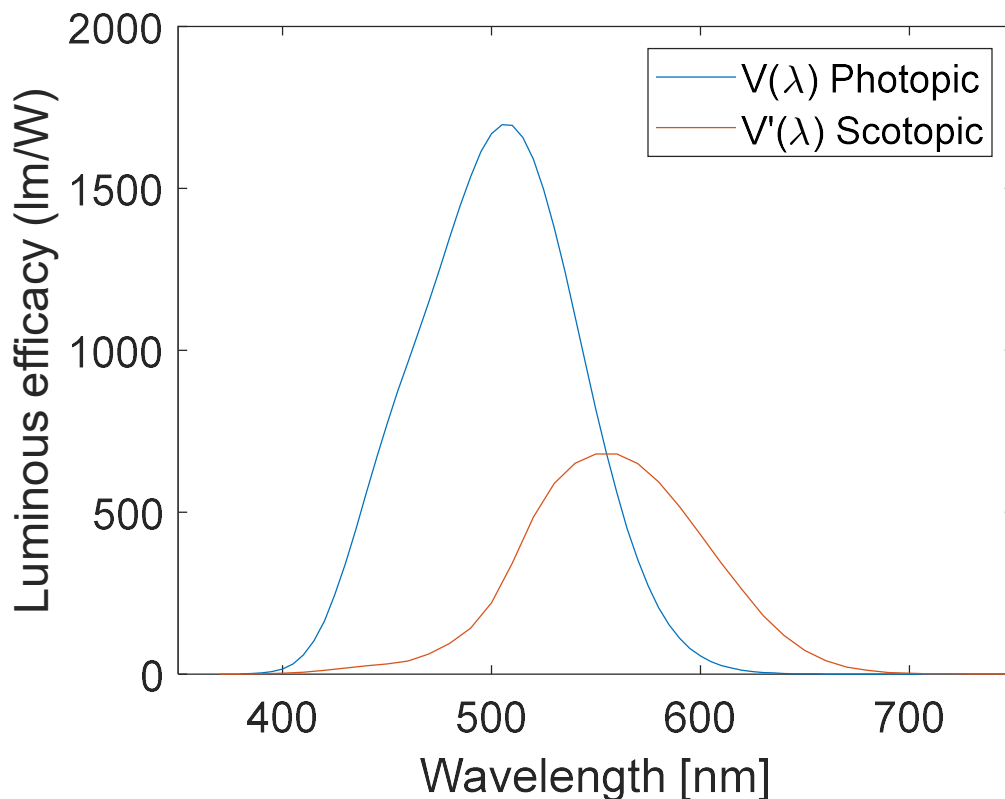


Fig. 1.3 Normalized responsivity spectra curves of the human cone cells, S, M, and L types; and

Rods

The photoreceptor's response defines the eye's response to all wavelengths in the visible spectrum, and the CIE in 1951 established the spectral luminous efficiency functions  $V(\lambda)$  and  $V'(\lambda)$ , creating three conditions; First of all, the photopic conditions are when the luminance is bigger than  $3 \text{ cd/m}^2$ . In this case, the rods are saturated, and only the cones are perceiving a visual signal. The second one is called the scotopic conditions, when the luminance is less than  $0.03 \text{ cd/m}^2$ , the light levels are too low to activate the cones, but the rods are responsive. The last one is the Mesopic conditions, which refer to the in-between state where both the rods and the cones are active. The spectral luminosity functions  $V(\lambda)$  and  $V'(\lambda)$  can be seen in the figure 1.4 <sup>(11,12,13,14)</sup>.



*Fig. 1.4 The spectral luminous efficiency function for photopic and scotopic vision.*

## 1.2.4 Colorimetry

### 1.2.4.1 Three-color matching

The three-color matching or trichromatic matching is the internationally accepted method in detriment of the three cones spectral sensitivity with the rod's effect because their curves are not known sufficiently. The CIE in 1931 defines the color-matching functions to be expressed in terms of the matching stimuli, R, G, and B. The amount of monochromatic red light needed for a match is represented by  $\bar{r}(\lambda)$ , while  $\bar{g}(\lambda)$  represents the amount of monochromatic green light, and  $\bar{b}(\lambda)$  represents the amount of monochromatic blue light needed for a match. The curves can be seen in the figure 1.6.

The trichromatic color theory update on the fact that color vision is the consequence of the three photoreceptor cells' signals. It was conducted to a color-matching experiment to show that any light can be matched by a mixture of three different primary lights. The necessary experimental arrangement for the trichromatic matching is shown in Figure 1.5. Observers view a bipartite field and adjust the three sources' intensities to match the colors in the two regions of the screen. The test color to be matched is seen in one half of the field of view, and, in the other half, the observer sees an additive mixture of beams of red, green, and blue light. The amounts of red, green, and blue light are then adjusted until the mixture matches the test color in brightness, hue, and colorfulness<sup>(11,14)</sup>:

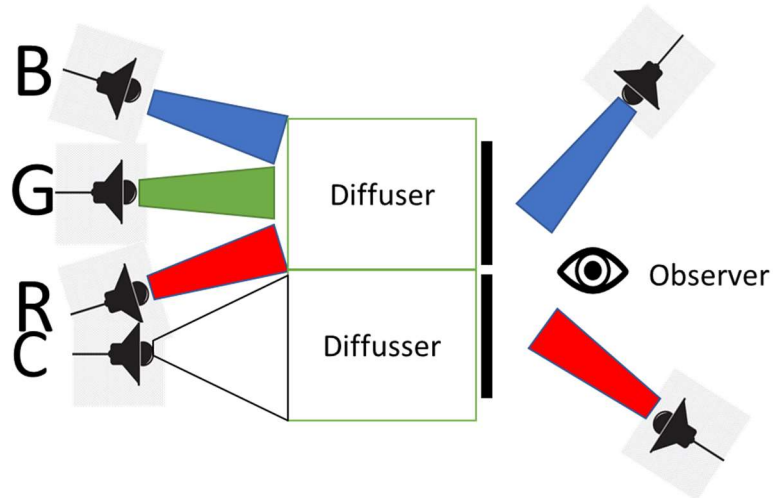


*Fig. 1.5 The Color-Matching Experiment. The R, G, and B are sources of red, green, and blue light, whose amounts can be adjusted; C is the light whose color is to be matched. The diffusers result in uniform fields for viewing by the observer.*

The three basic perceptual attributes of a color are its hue, its brightness, and its colorfulness, which are described as follows.

**Brightness:** An attribute of a visual perception according to which an area appears to exhibit more or less light.

**Hue:** An attribute of a visual perception according to which an area appears to be similar to one, or proportions of two, of the perceived colors red, yellow, green, and blue.

**Colorfulness:** An attribute of a visual perception according to which an area appears to exhibit more or less of its hue (CIE,2011) <sup>(14)</sup>.

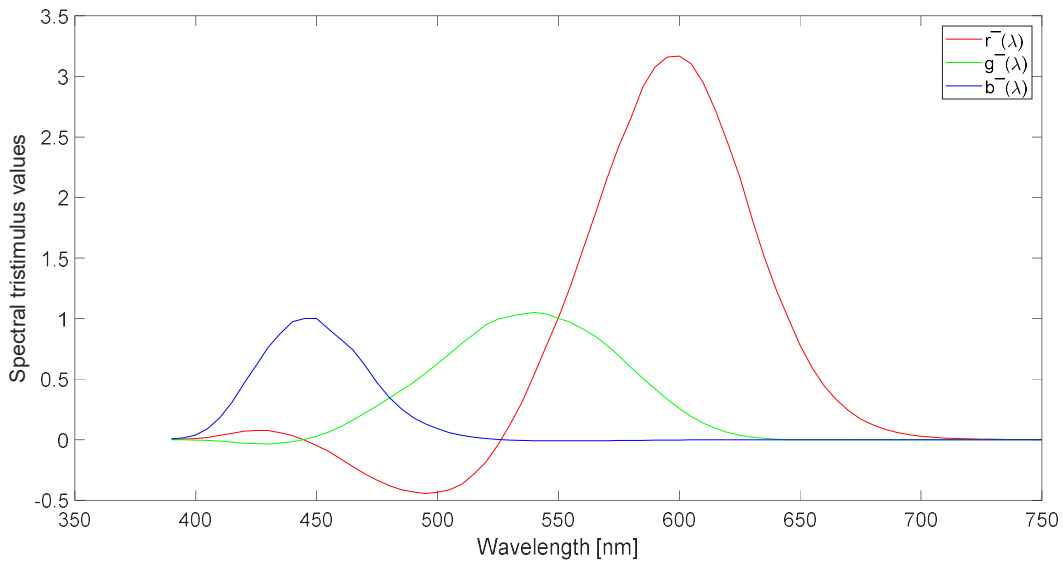


Fig. 1.6 Trichromatic matching functions obtained by Stiles 10.

#### 1.2.4.2 Tristimulus values

The tristimulus values, R, G, and B, are “the amounts of the three reference matching stimuli required to give a match to the color (or light) considered,” then the  $\bar{r}(\lambda)$  curve shows the amount of R needed for a match to be made for each wavelength of the spectrum; and the  $\bar{g}(\lambda)$  and  $\bar{b}(\lambda)$  curves show the amounts of G and B respectively and they are obtained from the color matching functions that are shown below <sup>(11,12,14)</sup>.

$$R = \int_{\lambda} \phi_{\lambda}(\lambda) \bar{r}(\lambda) d\lambda \quad \text{equation 9}$$

$$G = \int_{\lambda} \phi_{\lambda}(\lambda) \bar{g}(\lambda) d\lambda \quad \text{equation 10}$$

$$B = \int_{\lambda} \phi_{\lambda}(\lambda) \bar{b}(\lambda) d\lambda \quad \text{equation 11}$$

$\phi_{\lambda}(\lambda)$  is the color stimulus function.

The CIE consider a set of tristimulus values  $\bar{x}(\lambda)$ ,  $\bar{y}(\lambda)$ , and  $\bar{z}(\lambda)$  instead of the tristimulus values R, G, and B to avoid negative values in color specifications. The new tristimulus values can be seen in the figure 1.7 and they are obtained by using following the equations:

$$\bar{x}(\lambda) = 2.768892 \bar{r}(\lambda) + 1.751748 \bar{g}(\lambda) + 1.130160 \bar{b}(\lambda) \quad \text{equation 12}$$

$$\bar{y}(\lambda) = 1.000000 \bar{r}(\lambda) + 4.590700 \bar{g}(\lambda) + 0.060100 \bar{b}(\lambda) \quad \text{equation 13}$$

$$\bar{z}(\lambda) = 0 + 0.056508 \bar{g}(\lambda) + 5.594292 \bar{b}(\lambda) \quad \text{equation 14}$$

where the tristimulus value  $\bar{y}(\lambda)$  is equal to the luminous efficiency function  $V(\lambda)$

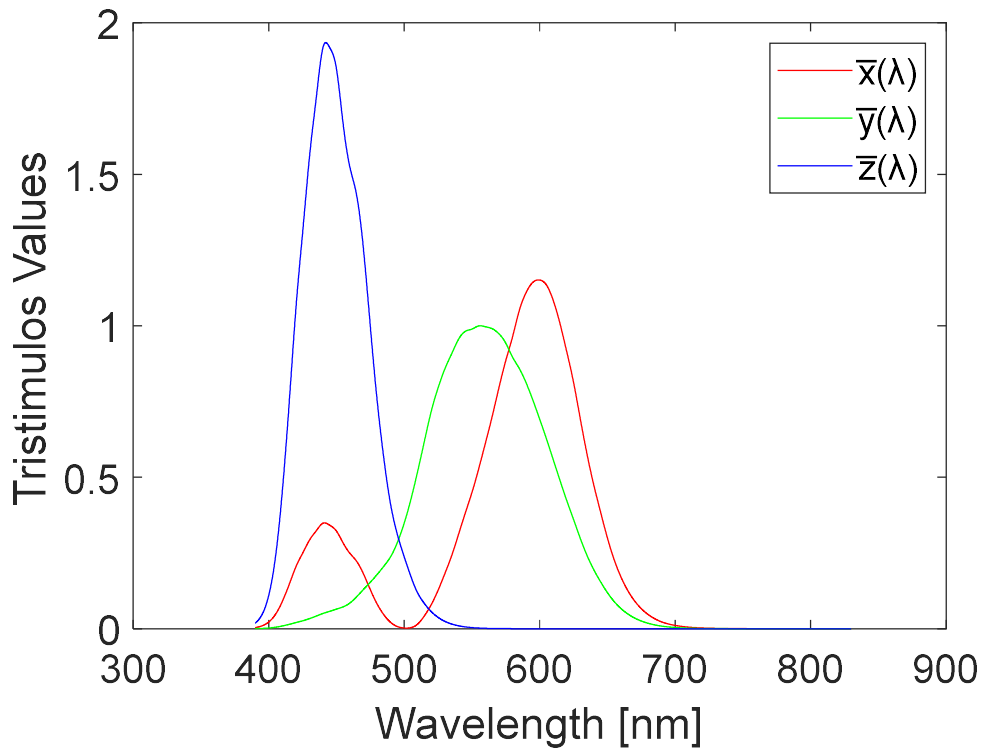


Fig. 1.7 The CIE 2° XYZ CMFs transformed CIE (2006) LMS cone fundamentals

The  $\bar{x}$ ,  $\bar{y}$ , and  $\bar{z}$  color matching functions shown in Figure 1.7 are called the CIE standard colorimetric observer. The CIE standard observer is commonly used in the colorimetric calculations to represent the human visual response to the colored stimuli.

### 1.2.4.3 Chromaticity

The tristimulus values can be derived to other measures that can correlate with perceptual attributes. The chromaticity coordinates are the calculations that relates relative magnitudes of the tristimulus values to important color attributes and they are shown in the following equations <sup>(11,12,14)</sup>.

$$X = \int_{\lambda} S(\lambda)\bar{x}(\lambda)d\lambda \quad \text{equation 15}$$

$$Y = \int_{\lambda} S(\lambda)\bar{y}(\lambda)d\lambda \quad \text{equation 16}$$

$$Z = \int_{\lambda} S(\lambda)\bar{z}(\lambda)d\lambda \quad \text{equation 17}$$

The chromaticity coordinates  $x$ ,  $y$  and  $z$  represent the relative amounts of the tristimulus values. Knowing the variables  $x$ ,  $y$ , and  $z$  is obtained from  $1 - x - y$ . Having only two variables becomes possible to construct a two-dimensional diagram called the chromaticity diagrams (the CIE 1931 color space diagram). This diagram shown in the figure 1.8 provides a sort of color map on which all colors' chromaticity can be plotted <sup>(11,12,14)</sup>.

$$x = \frac{X}{X+Y+Z} \quad \text{equation 18}$$

$$y = \frac{Y}{X+Y+Z} \quad \text{equation 19}$$

$$z = \frac{Z}{X+Y+Z} \quad \text{equation 20}$$



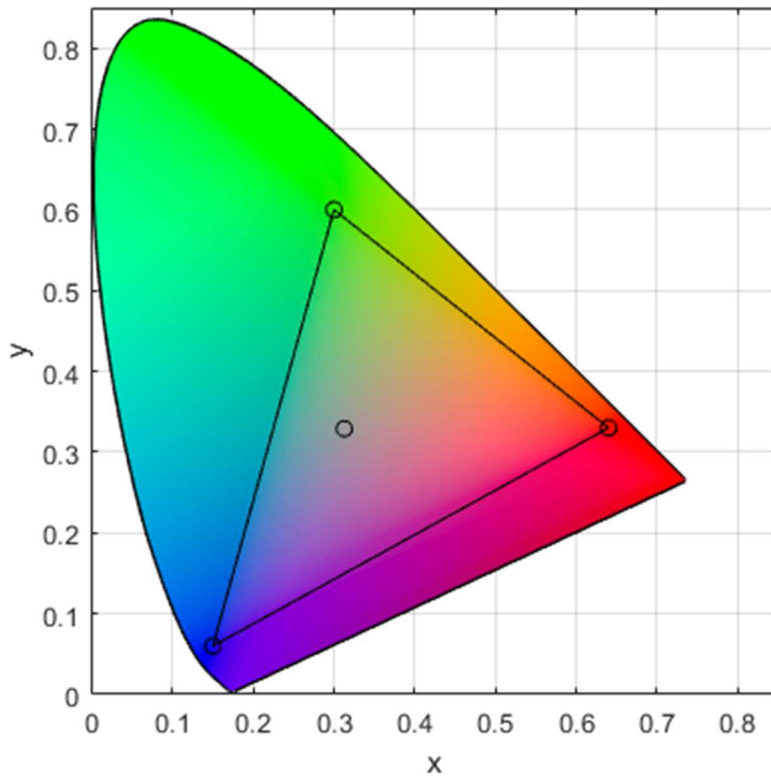


*Fig. 1.8 The CIE 1931 (x, y) Chromaticity Diagram, the colored boundary line represents the coordinates of intense monochromatic light. White light is a line in the center used as a reference point. The equal-energy point is located at the center and has the coordinates  $(x, y) = (1/3, 1/3)$ .*

#### 1.2.4.4 Color Mixing

Additive color mixing is the mathematical method for creating a color by mixing two or more colored light sources at varying wavelengths. In the additive mixing, a new color can be achieved by superimposing different lights, projecting them in succession at a high frequency, or viewing them in adjacent pixels close enough as in television screens. The final mixture is the sum of the sources by superimposing the individual light spectra. Figure 1.9 shows an example of the spectral representation of the color mixing <sup>(11,12)</sup>.

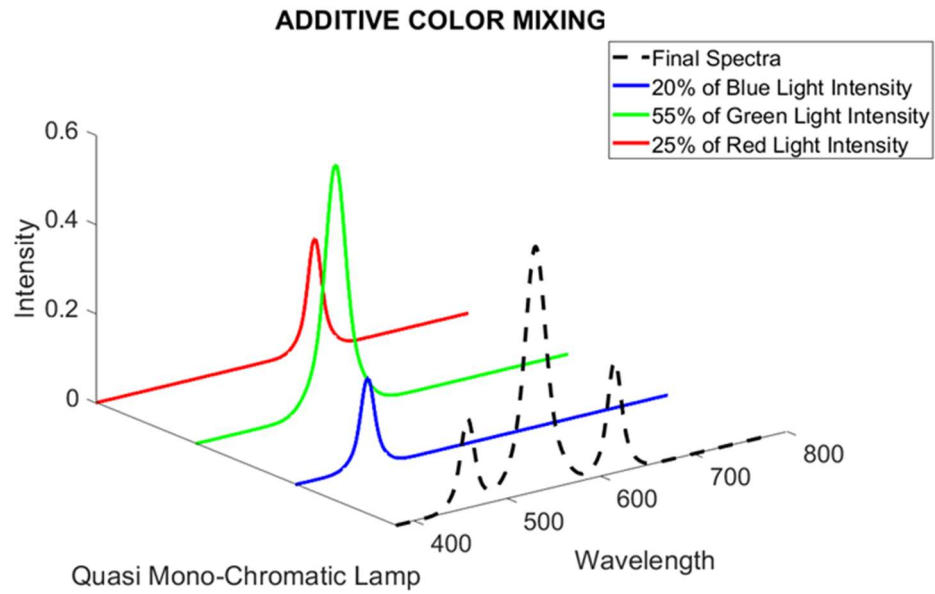


*Fig. 1.9 Red, blue, and green spectral primary colors. The dashed line is the sum or the superimposition of the three primary colors, which represent the mixed color or the final spectrum.*

## 1.3 Literature Review

This section describes the progress of the technologies involved in this dissertation. The LEDs and the cathodoluminescent phosphor lamps are explained in terms of the monochromatic light sources and how they can be optimized to generate many different desirable SPDs in the fields of the plant growth, the preserving museum artifacts, and the creation of color spaces.

### 1.3.1.- Light Source Selection, Fabrication and Spectral Characterizations

One of the main concerns in terms of the SPD is the generation of the artificial white color light emission that accomplishes a good color representation, similar to daylight; or in other words, exhibits qualities closest to daylight with a high color rendering index (CRI), a matched correlated color temperature (CCT), and a color quality scale (CQS) <sup>(15,16)</sup>. New investigations about how light affects the inorganic and organic materials has increased the number of desired SPD as demanded by different fields <sup>(2-10,17,18)</sup>. The creation of a lamp with the desirable SPD can be obtained by different options. One of them is to produce a wide SPD, and then a range of wavelength not desirable can be filtered usually by adding an absorptive layer in the lamp's glass <sup>(2)</sup>. The problem of this technique is the reduction in the energy's efficiency since some light already produced will be filtered out. Another option is to emulate the desirable SPD <sup>(3-6,8)</sup> by combining quasi-monochromatic lamps at various intensities.

The desired SPDs studied in this work are produced to target the fields listed below and explained in this section:

1. Preserving Museum Artifacts

2. Plant Growth
3. Color Quality Indexes
  - a. CRI
  - b. CCT
  - c. Chromaticity diagram.

#### 1.3.1.1 Preserving Museum Artifacts

The investigation in “SSL Adoption by Museums: Survey Results, Analysis, and Recommendations <sup>(15)</sup>” explains the SPD's relevance and the importance on preserving museum artifacts. In this report, many investigations and opinions from the professionals responsible for conserving museum collections placed the SPD of light as the primary concern for selecting the illumination. The concerns are about the potential damage to the museum artifacts by the light sources; and it is described by the absorption of photon energy by the substances. However, light absorption does not guarantee that a chemical change will be produced; when the photon is absorbed, the molecule is in an excited electronic state, and several distinct events can happen in this condition. In a molecule, a chemical change is produced when a bond between its constituent particles breaks owing to the photon-induced excited state <sup>(18)</sup>.

Determining an object's significant molecular change can be predicted by knowing whether the light energy is absorbed and the quantum yield for the subsequent photochemical reaction. The absorption information is determined by comparing the light source's emission spectrum with the reflected spectrum from the object; the difference tells us if any energy is absorbed. The photochemical reaction is inferred from the results of quantitative photochemical experiments <sup>(18)</sup>.

The Commission Internationale de L'Eclairage (CIE) is the organization accepted as representing the best authority on the subject matter of light and lighting. They have provided recommendations to control the damage to the artifact in a museum setting. One of the most vital suggestions is eliminating all optical radiation below 400 nm. They also recommended maintaining the illuminance below 50 lx for materials that are moderately or highly responsive to damage, and for materials with low responsivity, they also recommended maintaining illuminance below 200 lx. For comparison, 100 lx is considered the standard illumination level of office space. Therefore, there is a considerable effort to create an optimal SPD profile that not only renders a high color quality representation but also offers low damage to the museum artifacts. Usually, such optimal SPDs can be achieved by using a combination of quasi-monochromatic light sources <sup>(2-5, 17)</sup>.

#### 1.3.1.2 Plant Growth Absorption Spectrum Mimicking Light Sources

Plant growth is another field in which a desirable SPD is required. The SPD emitted by the source will be used to drive photosynthesis reactions through what is called the photosynthesis-action spectrum (PAS). It profoundly influences plant morphology, physiology, and development—changes in the spectral composition of light impact processes ranging from photosynthesis to secondary metabolism. Three spectral components construct the PAS; the first and more significant is chlorophyll-a. However, plant growth needs chlorophyll-b to assist light absorption for the chlorophyll-a; the carotenoids also assist light absorption and further release any excessive photonic energy that might damage the chlorophyll-a and the chlorophyll-b. The ideal light for plant growth should have at least an emissive spectrum

covering those three pigments. Growing plants efficiently requires that the artificial light source's emissive spectrum closely matches the three pigments in the (PAS) observed from a chloroplast <sup>(7,8)</sup>.

The ideal lighting device should also have a high degree of design freedom in spectrum-tailoring so that the resulting spectrum can better match chlorophyll-a, chlorophyll-b, and carotenoids. There are also investigations using a narrow range of visible light to improve the plant's specific characteristics, such as roots, stems, leaves. The effects of adding **far-red, red, blue or UV** improve the greenhouse condition in other areas, such as plant defense against arthropod herbivores and plant–arthropod interactions and arthropod behavior <sup>(19)</sup>.

### 1.3.2 Monochromatic sources

The combination of quasi-monochromatic (QM) light sources has been used to obtain the lamps with desirable SPDs' on various fields mentioned previously. The LEDs and cathodoluminescent phosphor lamps are generally used as QMLSs; their functioning and some of the latest improvements are described in this section.

#### 1.3.2.1 Light Emitting Diodes sources

The development of inorganic LED semiconductor materials and device structures has been driven since the 1960s, but it was not until the 1990s that bright-blue and saturated green LEDs were achieved <sup>(20,21)</sup>. Today, all the visible spectrum is achieved by using green and red Quantum Dots (QDs) as the down-converter <sup>(22,23)</sup>. Commercial inorganic LEDs typically have an efficiency greater than 20% <sup>(22)</sup>; The red and blue inorganic LEDs with high efficiency an external

quantum efficiency (EQE) greater than 45% for III-V and III-nitride LEDs. The current AlGaInP-based LEDs have emission levels as high as 168 lm/W<sup>(22,23,24)</sup>. Moreover, the colloidal quantum dots (QDs) are promising emissive materials due to their easily tunable wavelengths, narrow emission profile (FWHM), high stability, and high quantum efficiency. This enables us to tune the emission content of light by controlling the size of QDs, from ultraviolet to infrared, within a single quantum-dot group<sup>(21,26)</sup>.

Driving LEDs can be done by the traditional DC-DC converters in which  $N$  number of voltage or current outputs require  $N$  number of DC-DC converters in parallel. Other driving circuits implement the SIMO technique in DC-DC converters to avoid using  $N$  number of converters. However,  $N$  number of inductors is required for each output<sup>(21,27)</sup>.

Even though the LEDs are promoted because of the electricity savings, however, the LED lamps' damage on the human health is one of the concerns. Many papers review the negative impact of the LED lighting on the human organism, such as the importance of near-infrared light or the light's influence in synchronizing the circadian rhythms<sup>(28,29)</sup>. All those impacts should be considered when selecting an SPD designed by using the LEDs.

The LEDs are solid-state lighting (SSL) semiconductor devices producing light by electroluminescence; photons' emission or release from a material in response to an electric current. The simplest LED p-n junction is illustrated in Figure 1.11. Light is emitted when electrons and holes that flow as majority carriers are injected across the junction and recombine at or near the junction, leading to the radiative recombination<sup>(30)</sup>.

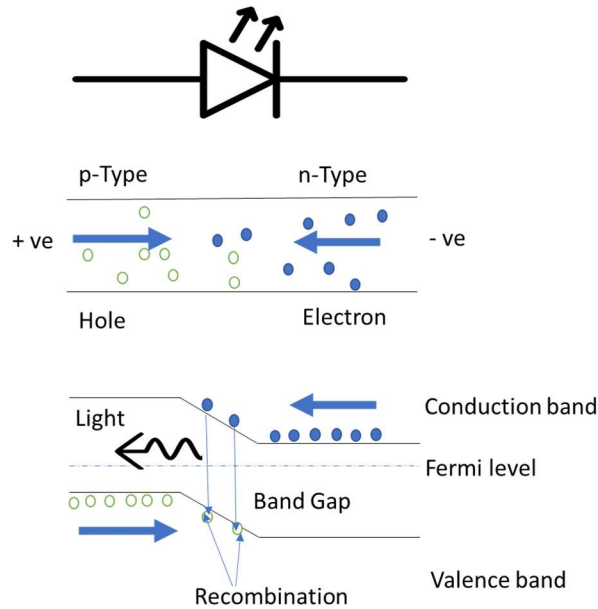


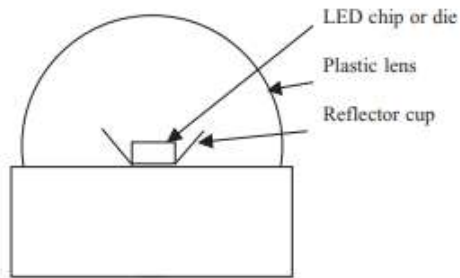
*Fig. 1.11 Forward-biased LED p-n junction. When one electron and one hole recombine near the junction one photon of light may be emitted.*

A direct-gap is often considered for radiative recombination in semiconductors due to its efficiency, and the most practical LEDs are not an exception. However, the indirect-gap semiconductors are also considered by using some other mechanisms that overcome the lower radiative recombination, which comes from a phonon required to satisfy momentum conservation <sup>(24)</sup>.

There are various LED device structures; however, the most common structure of a small LED showing both the packaging and the semiconductor die is illustrated in Figure 1.12. Since the light emission is from the sides and the front of the die, a reflective cup allows the light to propagate forwards and through a molded epoxy polymer lens <sup>(31,32)</sup>.



A



B

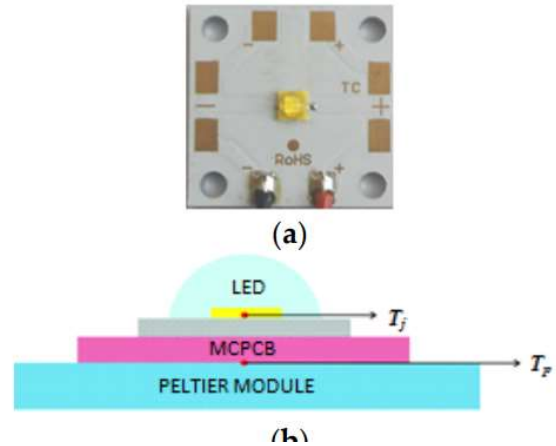


*Fig. 1.12 LED Structure, the radiation pattern is determined by packaging, the combination of the die emission, the reflector cup and the shape and refractive index of the polymer lens. a) LED structure, b) LED Structure from datasheet Cree® XLamp® XP-C LEDs.*

The spectral emission of LED sources is usually narrow band with a Full Width at Half Maximum (FWHM) around 20 nm, and its spectrum depends on the semiconductor materials or the dimension in the case of an LED Dot. Nowadays, all the individual colors can be achieved, and the white LEDs can be manufactured by mixing the multi-color LEDs, coating a blue LED sources with a yellow phosphor, or converting UV to visible radiation with blue and yellow (or red, green, and blue) phosphors. The spectral power distributions of a phosphor-coated LED (pcLED) and a red, green, and blue (RGB) LEDs are shown in Figure 1.13 <sup>(22, 24, 26)</sup>.

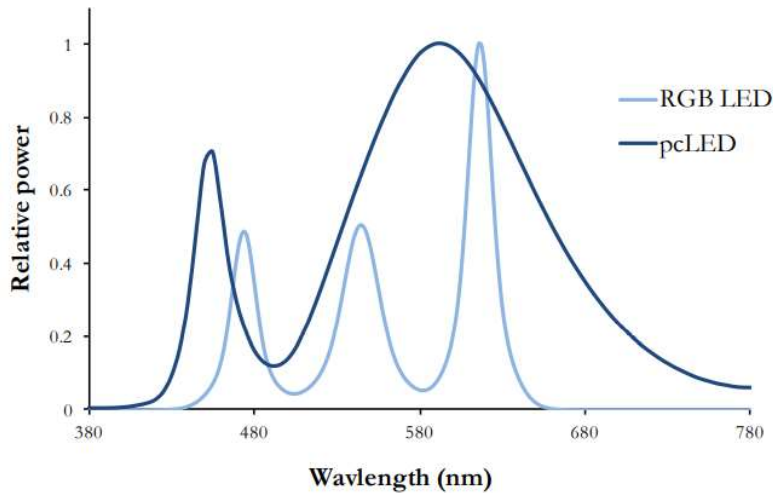


Fig. 1.13 The spectral power distribution of a phosphor-coated LED (darker blue line) and a three color LED with its peak wavelengths at 473 nm, 544 nm, and 616 nm (lighter blue line)

Thermal Characteristic

One of the limitations of even faster LEDs is the high temperature of the semiconductor junction  $T_j$ , which reduce the e-h pair to light conversion and the luminous flux  $\Phi$ ; and negatively affects the current-voltage characteristic of the LED sources as shown in Figure 1.14. The mentioned thermal problems are increased when they are located near each other due to the thermal interaction since they need to be grouped in a panel to accomplish the required luminous flux  $\Phi$  <sup>(33)</sup>.

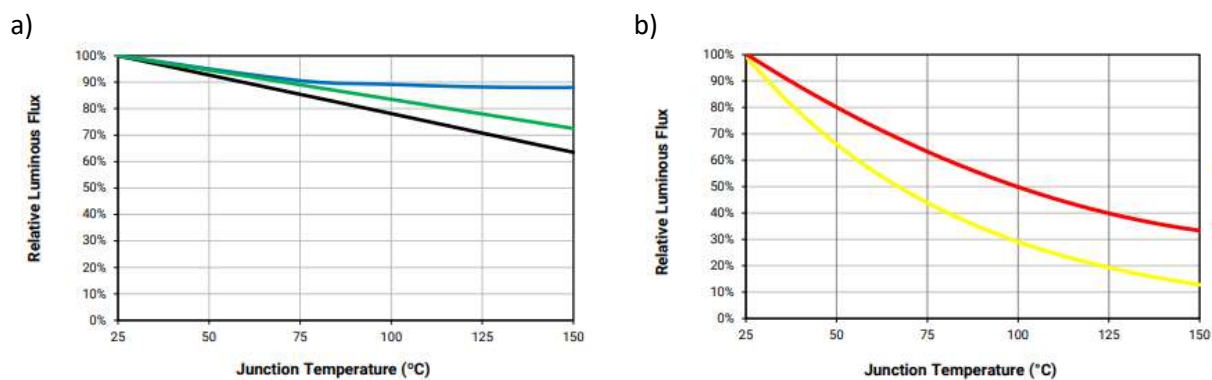


Fig. 1.14 Relative flux vs junction temperature ( $I_f=350$  mA), a) White, Blue and Green LEDs b) Amber (Red-Orange) and Red LEDs. datasheet Cree® XLamp® XP-C LEDs

As the junction temperature increases, its influence on the energy band gap begins to dominate, and the peak wavelength shifts linearly towards longer wavelengths. It produces a change in the spectrum of the LED source not only in terms of the luminous flux  $\Phi$ , but also in the color temperature called correlated color temperature (CCT), and the color rendering index (CRI) <sup>(33)</sup>.

#### 1.3.2.1 Cathodoluminescence Phosphor Lamps

The Cathodoluminescent phosphor light sources are based on the phosphorescent materials that emit light when they are impacted by electron beams. The SPD produced covers a broader wavelength spectrum range than LEDs. This method of light emission is used for clean and high-efficiency light source devices, and most of the characteristics can be improved by using the field emission technology enabled by a high vacuum, a high acceleration voltage, and implementation of cold cathodes <sup>(34, 35, 36, 37)</sup>.

The cathodoluminescence phosphor (CLP) materials are composed mainly of an inert host lattice. They should be transparent enough in the visible wavelength range to transmit the visible light to the powder crystallites' surface. The second component is the impurities that activate the crystal to luminescence, referred to as an activator. The activators will create localized energy levels similar to a bandgap, providing effective recombination paths for the excited electrons and holes. In practice, the primary properties of CL phosphor are characterized by intensity and color. These characteristics are determined by the nature of luminescence centers (activators) doped in the host crystals <sup>(34,38,39,40,41)</sup>.

The CLP lighting phenomenon is the result of the penetration of a primary electron beam into the phosphor, which is shown in Figure 1.15.

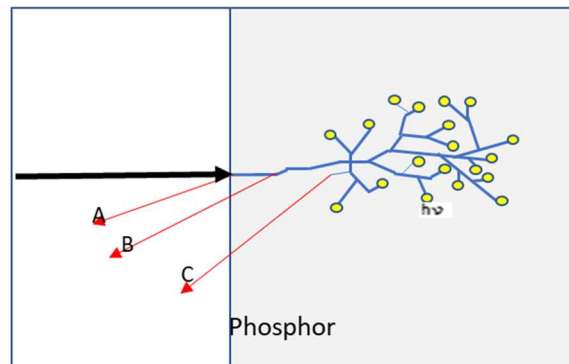


*Fig. 1.15 Schematic representation of processes in cathodoluminescence  
A) back-scattered primary electrons, B) back-scattered primary electrons with some energy loss, C) low-velocity secondary electron emission,  $h\nu$ ) luminescence event, light emission<sup>(34)</sup>*

Figure 1.15 shows an energetic electron accelerated by high voltage entering an inorganic crystal. The impact produces hundreds of free electrons and holes along the path of the incident electron. The intensity of the light produced will depend on the energy available when the exciting secondary electrons return to their ground states via suitable radiative transitions, which can be explained by the model of luminescent transitions of the phosphor material <sup>(34)</sup>.

The Zinc sulfide can be used to explain a simplified model for the mechanism of the cathode excitation. The unexcited state of the crystal is shown in Figure 1.16. The impurity state represents a level of the "activator" element such as Cu and Ag activators in ZnS:Cu, Ag, and ZnS:Ag, Cl phosphors. The activators will create localized energy levels in the bandgap, as represented by transitions (b), (c), and (d) in Figure 1.16. These transitions, overwhelmingly of

the direct transition type (a), emit light whose photon energy is smaller than the bandgap in accordance with the depths of these levels <sup>(38)</sup>.

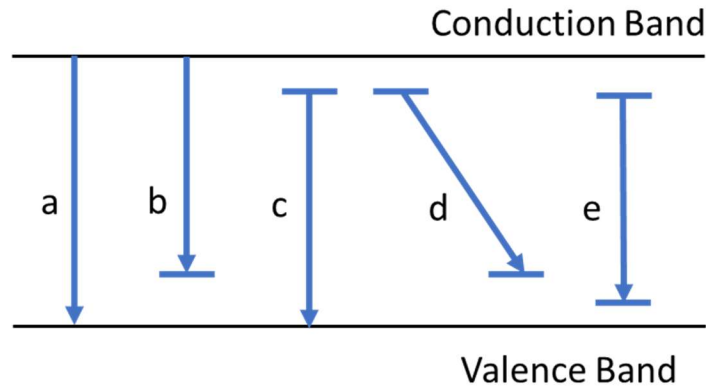


*Fig. 1.16 Models of luminescent transitions. (a) Direct recombination of a free electron and a hole (band-to-band transition); (b) transition of a free electron to an acceptor level (c) recombination transition of a donor electron with a free hole (d) transition between a donor and an acceptor (e) transition within a localized luminescent center<sup>(38)</sup>.*

The spectral emission of the CLP is usually wider than LEDs with a FWHM values broader than 50nm for QM materials, and its spectrum depends on the semiconductor materials. As an example, the nitride phosphor is used to create white light in Field Emission Lamps (FEL) devices, its high stability and reliability properties against the electron bombardment made it promising for flat FELs, their SPD can be seen in Figure 1.17. The CLP emission maximum and the full width at half maximum (FWHM) are 471 and 63 nm for AlN:Eu<sup>2+</sup>, 531 and 55 nm for  $\beta$ -sialon:Eu<sup>2+</sup>, 592 and 99 nm for Ca- $\alpha$ -sialon:Eu<sup>2+</sup>, and 625 nm and 81 nm for CaAlSiN<sub>3</sub>:Eu<sup>2+</sup>, respectively <sup>(41)</sup>.

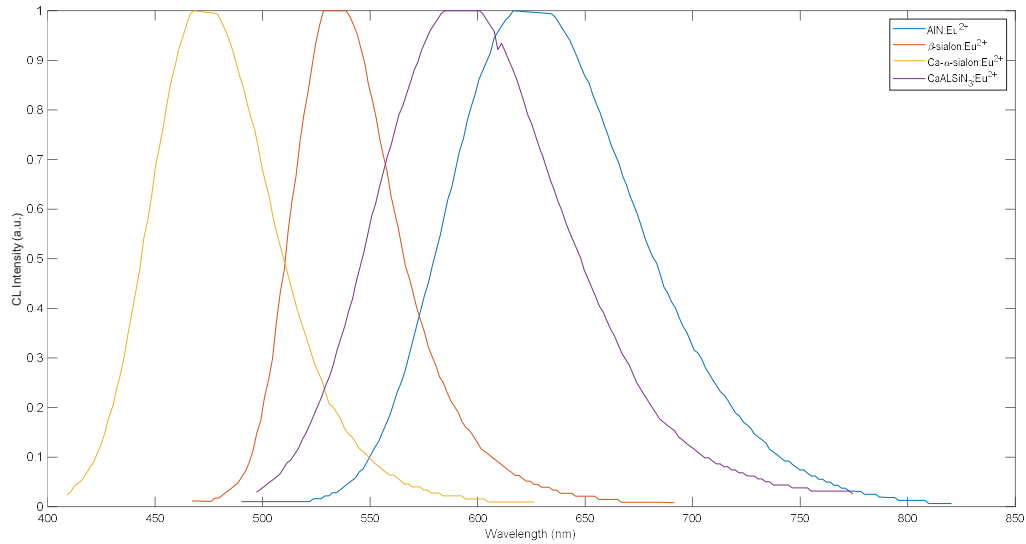
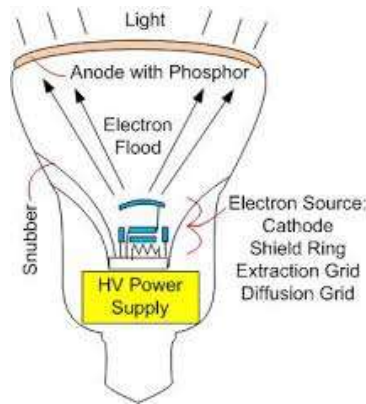


Fig. 1.17 Individual spectral power distribution of  $\text{AlN:Eu}^{2+}$ ,  $\beta\text{-sialon:Eu}^{2+}$ ,  $\text{Ca-}\alpha\text{-sialon:Eu}^{2+}$  and  $\text{CaAlSiN}_3\text{:Eu}^{2+}$  <sup>(41)</sup>.

A warm white light with the color temperature of 3,430 K can be achieved with the blue to yellow ratio of 0.65: 0.35. The color rendering index (Ra) varies in the range of 73 – 77. Much higher color rendering index of 93-96 can be achieved by replacing  $\text{Ca-}\alpha\text{-sialon:Eu}^{2+}$  with  $\beta\text{-sialon:Eu}^{2+}$  and  $\text{CaAlSiN}_3\text{:Eu}^{2+}$ , but sacrificing the luminous efficacy of the white FELs <sup>(41)</sup>.

Figure 1.18 shows the schematic of the commercial Vu1 light bulb with one of the structures of the cathodoluminescent phosphor lamps. The components are a vacuum envelope pumped using a getter, a cathode that emits a “flood” of electrons, uniformly accelerated toward the inner surface of the envelope on which the CL phosphors are applied. The electron optics restrict the flow of electrons to the phosphor layer, which has a reflective layer or conduction layer, to emit light outwards and collect the excess of the electron as the drain, respectively <sup>(37)</sup>.



*Fig. 1.18 Schematic of the Vu1 light bulb*

The power supply has high-voltage output and the total electron current is maintained such that the power density at the phosphor is low producing an efficient lamp <sup>(37)</sup>.

Another structure that shows significant improvements for the cathodoluminescence lamps is implemented by a field emission cold cathode instead of a thermionic. Figure 1.19 shows the field emission lamp configuration. It can have advantages such as the use of ITO or FTO transparent conductor layer instead of aluminum layer in the anode that conduct the electron accumulation out of the phosphor layer. This FEL structure also reduces the size of the device and exhibited excellent field emission properties with a minimum extraction field of 1.7 V/ m and good uniformity. The luminance characteristics were also excellent, with a white CLP being excited up to approximately 12,000 cd/m<sup>2</sup>; and the anode allocates different phosphor color powder achieving a variety of colors producing high CRI (CRI>90) <sup>(35, 36)</sup>.

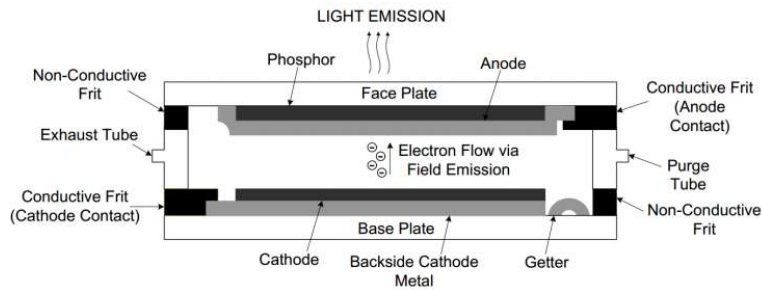


*Fig. 1.19 Cross-sectional view of FEL schematic.*

Another improvement for a phosphor cathodoluminescent lamp is the implementation of high voltage pulse excitation instead of DC for the accelerating voltage, which shows an improvement of 30% by avoiding the saturation condition in the poorly conducting phosphors (42, 43).

### 1.3 Genetics algorithms

This study under this dissertation aims to find the best combination of QMLSs to fit the desired SPD profiles. Then the different parameters of a set of single lamps has to be chosen, which requires considerable computational effort because of the infinite options that should be evaluated. This problem will be discussed in the section 2.4. where we produce overdetermined equations, and they have no exact solution in the classical sense (44).

This problem can be approximately solved with the optimization techniques, such as the evolutionary algorithms, one of the most popular of which is the Genetic Algorithms (GA). Other evolutionary algorithms are Particle Swarm Optimizations (PSOs), Ant Colony (AC), Simulated Annealing (SA), Differential Evolution (DE), Immune Algorithms (IA), Artificial Bee Colony (ABC), and Firefly Algorithm (FA) (45).



GA is a method for optimizing the search for problems based on the probability genetics selection principle. It is analogous to biology for chromosomes. This model consists of three essential elements that are explained below:

- Selection: A chromosome will be in a format that holds information related to the solution. The selection will be made by a fitness function that will keep the good exponents to influence the future generations.
- Crossover: Crossover functions swap portions of genes from the parent chromosomes which produces the offspring for the next generation.
- Mutation: It changes parts of one solution randomly, which increases the diversity of the population and provides a mechanism for escaping from a local optimum.

The GA code is a solution to a given problem in strings called chromosomes. The potential solution represented by each chromosome is evaluated according to a fitness function. The fitness function determines which chromosomes are selected to propagate the values of their parameters through subsequent generations. The new generation, analogous to children, is produced by three main operators: selection, crossover, and mutation. This process leads to generating new offspring and recursively continues replicating for multiple generations. The process is concluded once a GA is the most suitable for the issues. Figure 1.20 shows the basic steps followed by a GA in a flowchart <sup>(46)</sup>.

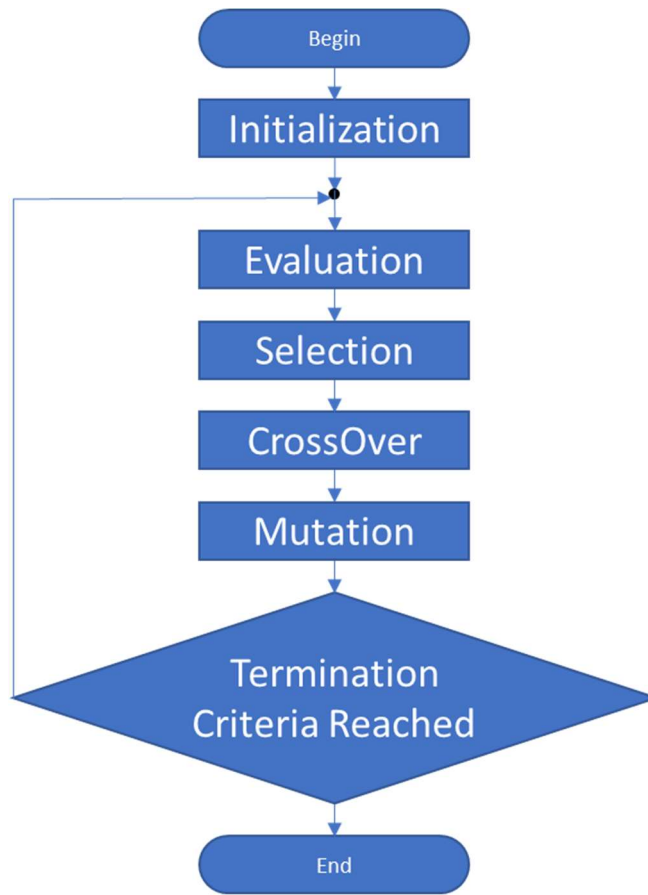


*Fig. 1.20 Flowchart of Genetics algorithms*

MATLAB provides the Global Optimization Toolbox functions that search for global solutions to multiple maxima or minima problems. The genetics algorithm repeatedly modifies a population of individual solutions. The GA selects individuals from the current population at each step and uses them as the parents to produce the children for the next generation. Over successive generations, the population "evolves" toward an optimal solution. Using these functions, the optimization tool to obtain the parameters for the QMLS is created, the chromosomes representation, fitness function and operators are explained in the section 2.4.

# Chapter 2

## Experimental Design and Modeling

This chapter describes the data collection and the model of creating a light source that mimics the desired SPD. Sections 2.1 and 2.2 explain the SPD measurements, the characterization of the LEDs, and the cathodoluminescence phosphor lamps. This part aims to collect the data by characterizing the QMLS behavior in terms of different excitation parameters. Consequently, obtained data is used to simulate the new SPD.

Section 2.3 describes the desired SPDs selected, and section 2.4 describes the model that optimizes the values of a set of QMLS coefficients that, when combined, mimic a desirable SPD.

### 2.1 SPD Characterization and Measurements for LEDs

Four LEDs were selected to create new SPD lamps to satisfy different requirements. The intensity vs. wavelength data for QMLSs is obtained by changing the individual excitation variables of the current and the voltage of each LED. The criteria for selecting the four LEDs take into account their lighting application, settings such as the wide viewing angle, symmetrical package, and range of peaks that can be covered <sup>(3)</sup>.

The four XP-C LEDs selected have peaks of 440 nm (Blue), 515 nm (Green), 590 nm (Amber) and 628 nm (Red), and the FWHM values are 20 nm, 43 nm, 14 nm and 15 nm at 300 mA respectively. The experiments were conducted with Ocean Optics Spectrometer (USB4000),

HCT-99, and luminance meter LS-100 (cd/m<sup>2</sup>). The SPD data collected by the spectrometer contains 3648 data points from 314.71 to 1052.64 nm with an increment of ~0.18nm. These values were interpolated using the polyfit and the polyval functions in MATLAB. Table 2.1 shows the specs of the LEDs utilized from their datasheets.

**Table 2.1** Wavelength peaks and Flux of LEDs taken by the datasheet.

Code	Color	Wavelength peak	Flux
XPCRED-L1-0000-00401	Red	639nm	51.7 flux lm
XPCGRN-L1-0000-00502	Green	523 nm	56.8 flux lm
XPCROY-L1-0000-00701	Blue	452 nm	250 flux lm
XPCAMB-L1-0000-00503	Amber	597 nm	56.8 flux lm

The LEDs and the PCB board were bought from the company called Cree LED CO. The electrical connections were completed at UC Davis. The Figure 2.1 shows the PCB board and the LEDs (31,32).

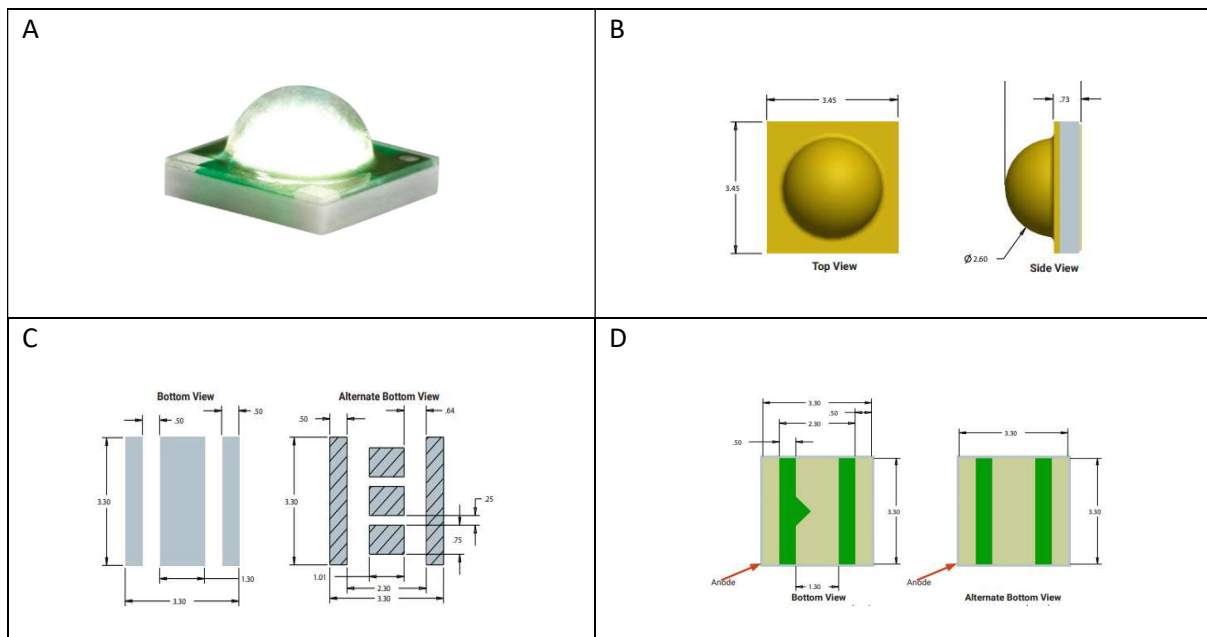


*Fig. 2.1 XP-C LEDs, all measurements are  $\pm 13\mu\text{m}$  unless otherwise indicated, a) photograph of the LED, b) top and side view sizes, c) PCB solder pad, d) Bottom and alternate bottom views.*

Varying currents were applied to the LEDs in the experiments, and the SPD results were collected and plotted with MATLAB. The SPD profiles at different current levels can be seen in Figure 2.2. Figure 2.3 shows the increment of Luminous flux vs current.

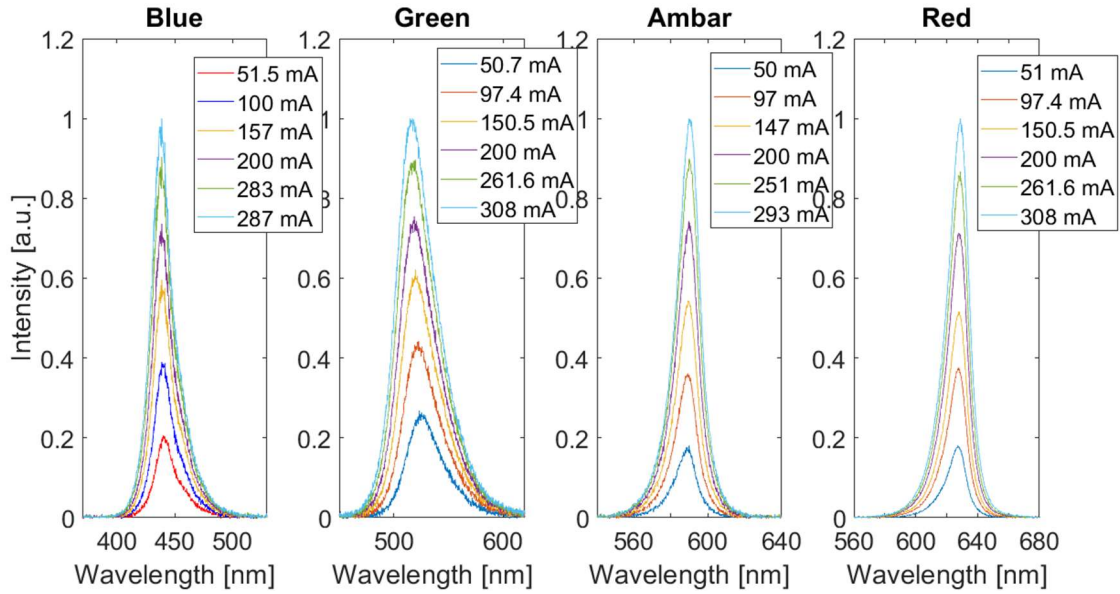


Fig. 2.2 SPDs of each of the four LEDs collected by using spectrometers.

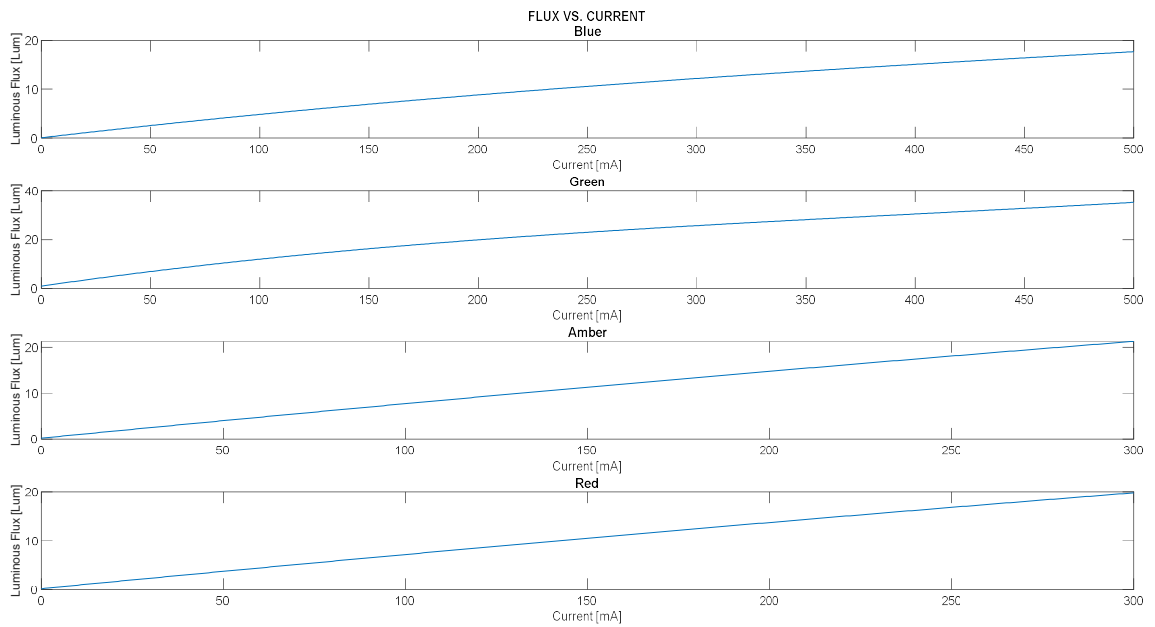


Fig. 2.3 Current vs. Luminous Flux of the four LEDs collected by using HCT-99.

## 2.2 SPD Characterization and Measurements for the Cathodoluminescent Phosphor Lamps

The process to obtain the SPD emitted by the cathodoluminescent phosphor materials was performed in a custom-built vacuum testing system in the Vacuum Microelectronic Laboratory at UC Davis. The vacuum testing system is composed of a pentode electron vacuum tube to create an electron beam and generate the cathodoluminescence emission on a phosphor-coated glass screen/window acting as the lamp. The system has the capability to change the cathodoluminescent phosphor samples, the accelerating voltage, the excitation current density; and allowing us to acquire the pressure of the vacuum system, the temperature on the screen, the intensity of the emitted light, and the SPD profile.

The system can be divided into 3 main components listed below and explained in the following subsections.

- a) The vacuum chamber
- b) The excitation variables
- c) The phosphor sample

### a.- The Chamber and Vacuum Testing System

The testing system uses a cryogenic pump which is cooled by the compressed helium. Figure 2.4 shows the layout of the system, and figure 2.5 shows a photograph of the vacuum system built in the Vacuum Microelectronics Laboratory at UC Davis.

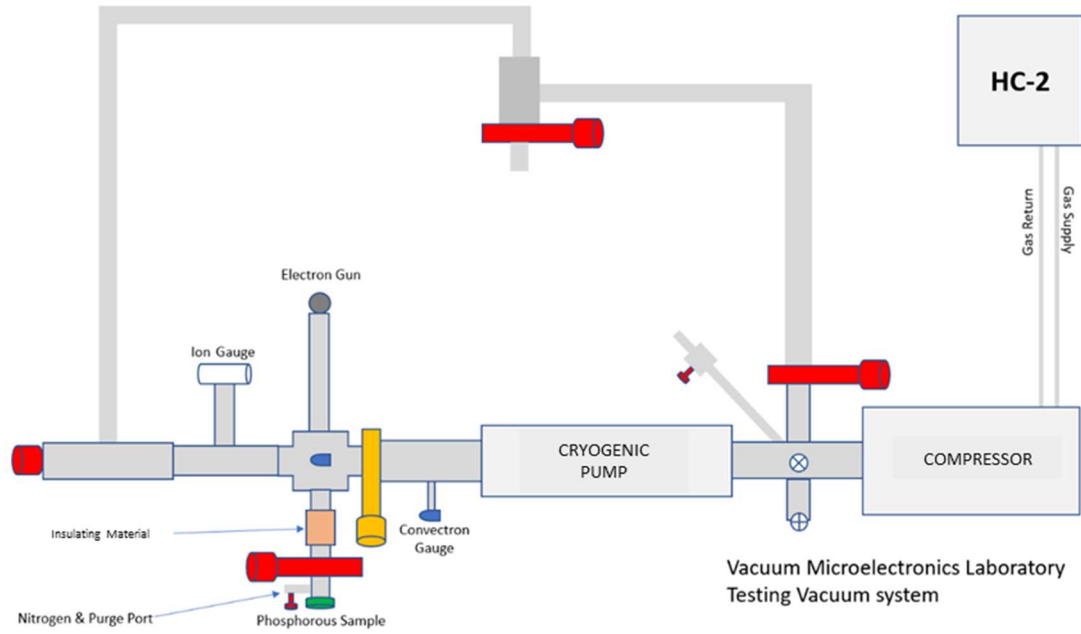


Fig. 2.4 Layout of the testing system

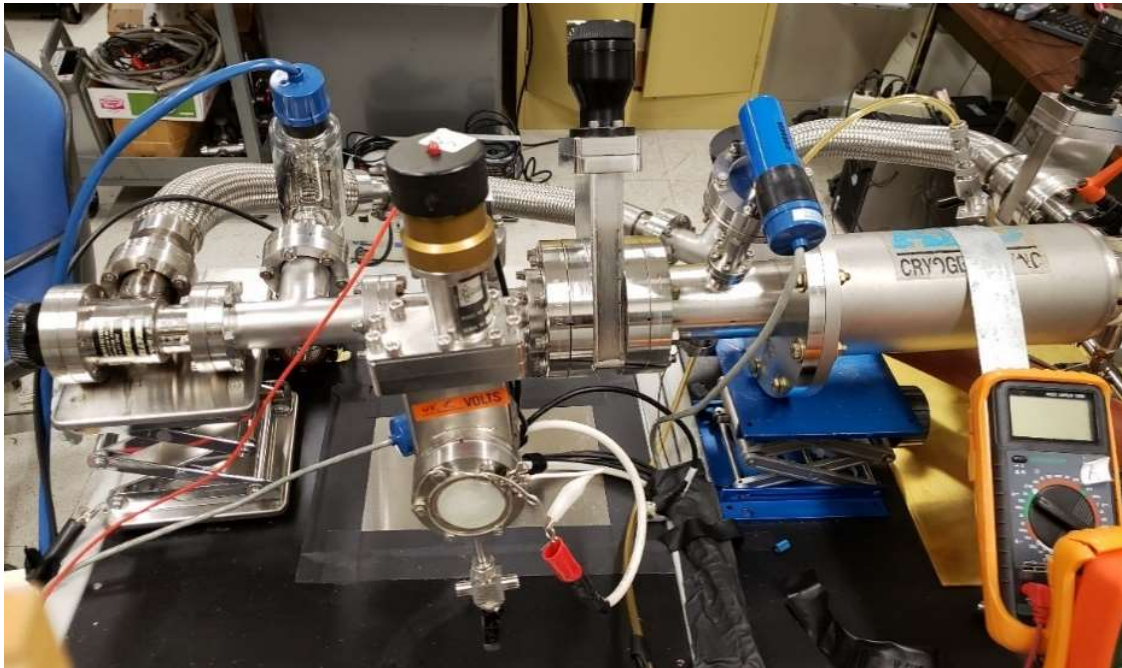


Fig. 2.5 Picture of the vacuum system built in the vacuum microelectronic laboratory.

The other components used in the vacuum testing system are a roughing pump, five valves, two convectron gauges, and an ion gauge.

The main requirements for the experiments are as follows:

- A maximum vacuum pressure of  $10^{-6}$  torr (the minimum pressure achieved is  $1.2 \cdot 10^{-7}$  torr).
- To be able to change the phosphor samples rapidly by the use of gate valves.
- To get the phosphor sample up to 15kV and the cathode to the ground.

b.- Electron Gun and Accelerating voltage:

The electron gun is the electrical component that produces an arrow collimated electron beam. When the cathode is heated, electrons can readily escape from its surface. These free electrons are accelerated in the vacuum by a high voltage on the anode. The hot plate of the cathode is connected to the ground. As soon as the electrons are emitted from the surface of the cathode, the high voltage on the anode attracts the electrons and accelerates them toward itself, thus to the phosphor layer which is located either behind or in front of the anode layer.

The cathode structure consists of barium oxide (BaO) coated disc (diameter 0.033", 0.84 mm) that is directly heated by a tungsten hairpin. The electron gun was fabricated by the E-company named E-beam Inc. in Beaverton, OR. Figure 2.6 shows the electrical circuit of the cathode, and Figure 2.7 shows a 3D figure of the cathode components.

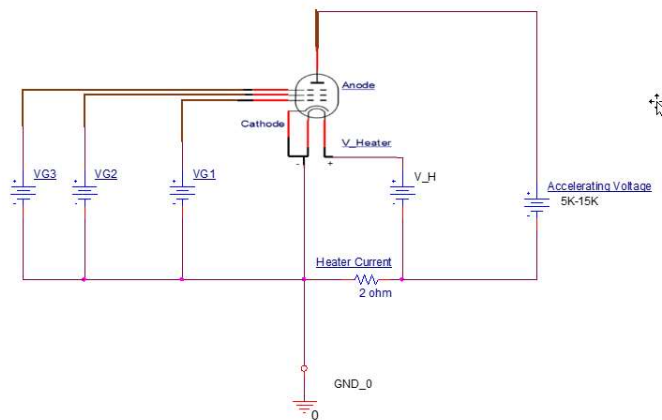
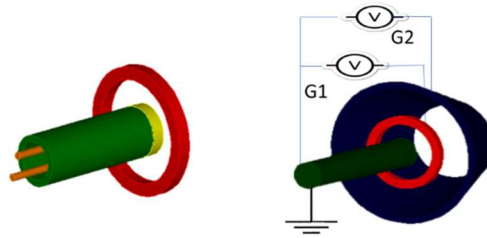


Fig. 2.6 Schematic diagram for the electron gun





*Fig. 2.7 3D figure for the cathode*

### c.- Phosphor Samples

The cathodoluminescent phosphor materials are sedimented on the glass discs with a diameters size of 2'', on which has there is a thin layer of Indium Tin Oxide (ITO) or Fluorinated Tin Oxide (FTO); the dominant materials used in the transparent conductive film (TCF) applications.

The sedimentation process can be summed up by the next steps:

- The phosphor settling process begins by choosing the phosphor quantity which is evaluated by taking a desired coating weight density ( $4.7\text{mg}\cdot\text{cm}^{-2}$ )
- The phosphor powder is mixed with Kasil (Potassium Silicate solution) and DI water by using a flask on a magnetic stirrer.
- The mixing vessel is placed in an ultrasonic agitation bath for 20s.
- A barium acetate diluted solution is placed in a settling vessel. The phosphor slurry should be taken directly from the ultrasonic agitation and immediately added to the settling vessel.

- Applying a high temperature to the deposit solidifies the silicate bonds. It has been observed that merely raising the temperature to 400°C and restoring back to room temperature fully solidifies the deposit. The figure 2.8 shows the cross-section of the layers of materials in the phosphor on a ITO-coated glass screen sample.

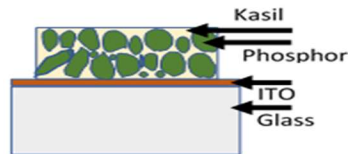


*Fig. 2.8 Schematic of a phosphor screen sample*

In the conducted experiments, the SPDs were collected and plotted by using the USB4000 spectrometer of Ocean Optics and MATLAB software, respectively. The SPD data contains 3648 data points from 314.71 to 1052.64 nm with an increment of  $\sim 0.18$ nm. These values were modified by interpolation using the polyfit and the polyval functions in Matlab. The SPD results of the CLP screens can be seen in the figures 2.9, 2.10, and 2.11.

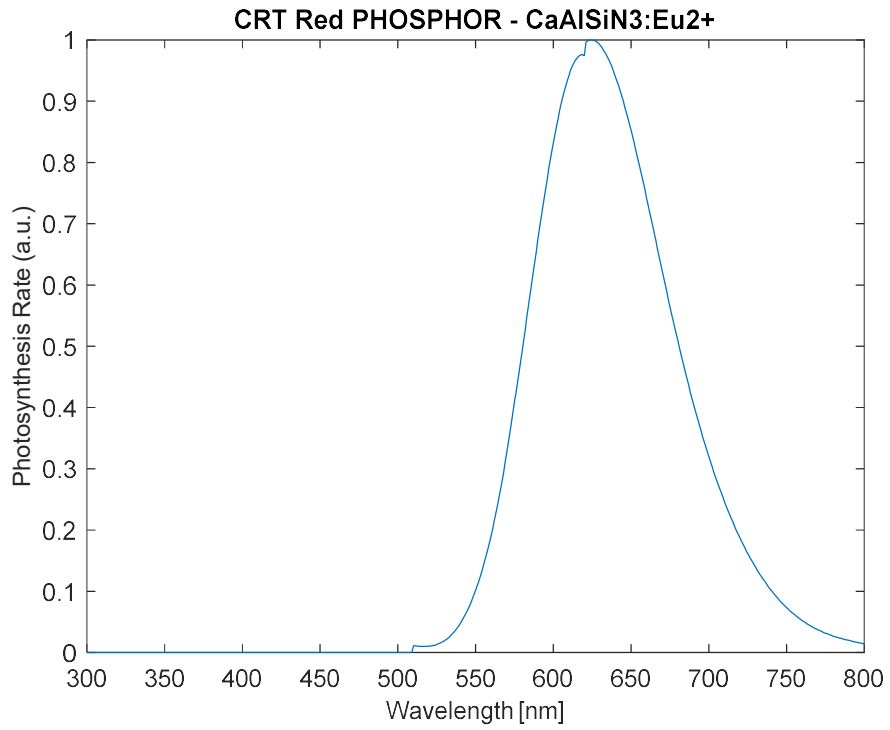


Fig. 2.9 SPD of the red cathodoluminescent phosphor.

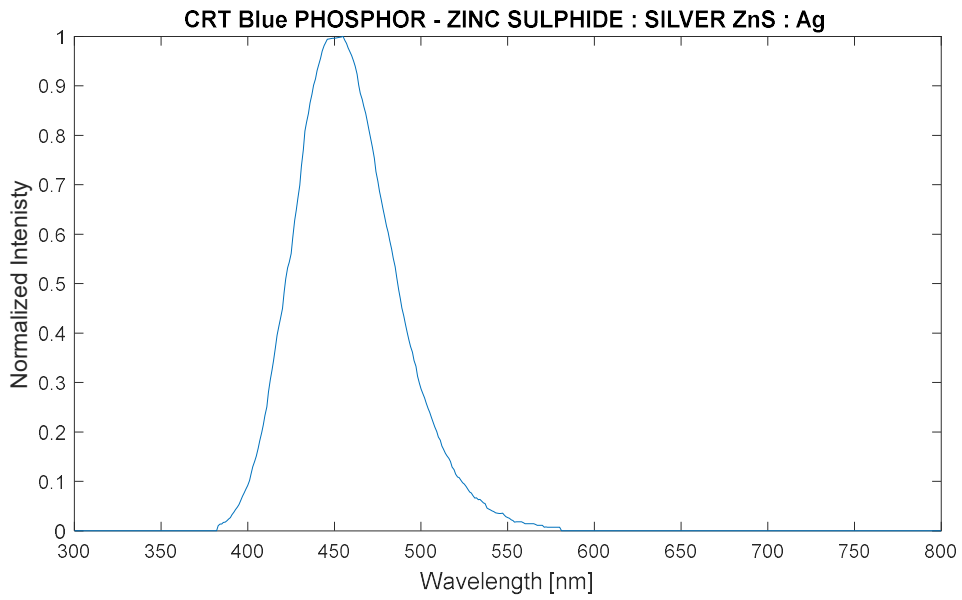
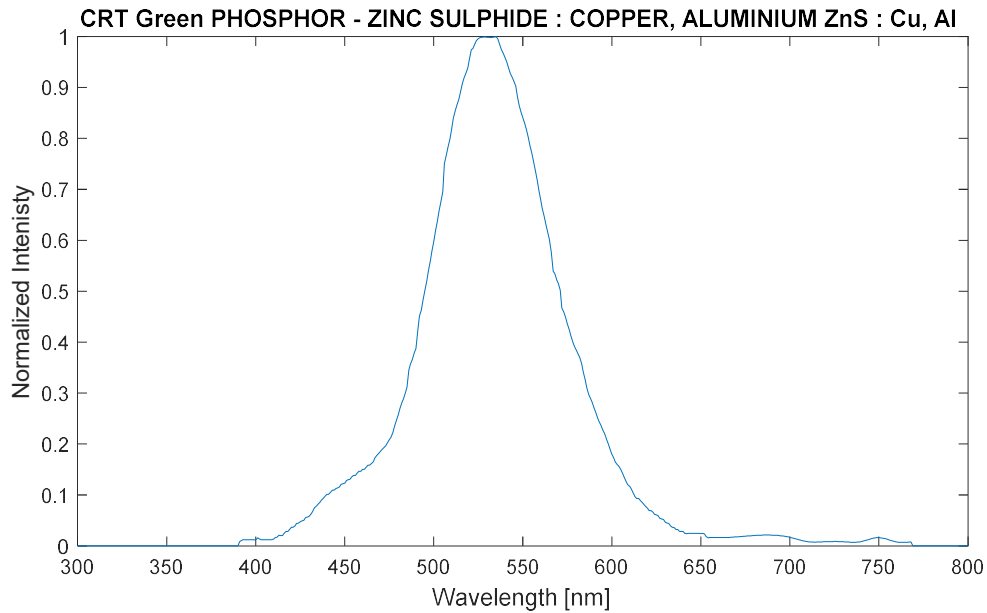


Fig. 2.10 SPD of the blue cathodoluminescent phosphor.



*Fig. 2.11 SPD of the green cathodoluminescent phosphor.*

## 2.3 Selection of the Desired SPDs

In this section, three desired SPDs were chosen from the literature. Those SPDs are used as the target for the simulation program to be mimicked. The two field of interest are the preserving museum artifacts and the plant growth. The relevance of the desired SPDs are described in subsection 2.3.1, 2.3.2, and 2.3.3.

The desired SPDs were scanned and digitalized using a software named un-scan-it 7.0. The data collected were properly processed on MATLAB by the `polyval` and the `polyfit` functions; and the plotted as shown in the figures 2.12, 2.13, and 2.14.

### 2.3.1 SPD required for preserving museum artifacts

The first desired SPD is taken from the publication titled “Lighting the World’s Treasures: Approaches to Safer Museum Lighting”, written by M. Delgado et al. in 2010 <sup>(2)</sup>. This optimized

SPD is calculated to reduce the photochemical degradation of old master drawings of art. This is achieved by improving the luminous efficiency of the spectral profile by reducing the light, which does not contribute to the brightness or the color perception, while also trying to maintain the color rendering quality.

This work aimed to create and test a methodology based on the improvement of the efficiency for the development of safer lighting for sensitive art and archival objects. There were two key parameters for the optimization: the luminous efficiency (L/W) and color rendering index (CRI).

Some of the considerations were highlighted in the following paragraphs.

- The optimization considered that the chromaticity was allowed to be possibly well off the blackbody curve.
- The spectral distribution may have unusual features and possess multiple cutoffs to enhance protection.
- The CCT was considered a significant quantity (if the illuminant chromaticity is far off the blackbody curve).
- The calculation of the CRI involved replacing the standard Munsell hue reference reflection set with the reflection spectra from a representative set of Old Master drawings (OMD). It is due to the eight Munsell color standards will produce saturation on the OMD.

Different optimal spectral profiles were obtained by optimizing for maximal L/W. The transmitted power decreased, and the transmission spectrum breaks into multiple bands. The

location and the number of the bands changed based on the reference lighting and the reference reflectance spectra.

Figure 2.12 shows the optimized SPD obtained in this paper. This spectrum was obtained by using a Sylvania 58562 brand lamp and using some materials to filter out the undesirable ranges of SPD. The SPD obtained is called “Mark 3” and produces the properties shown in Table 2.2 and Table 2.3

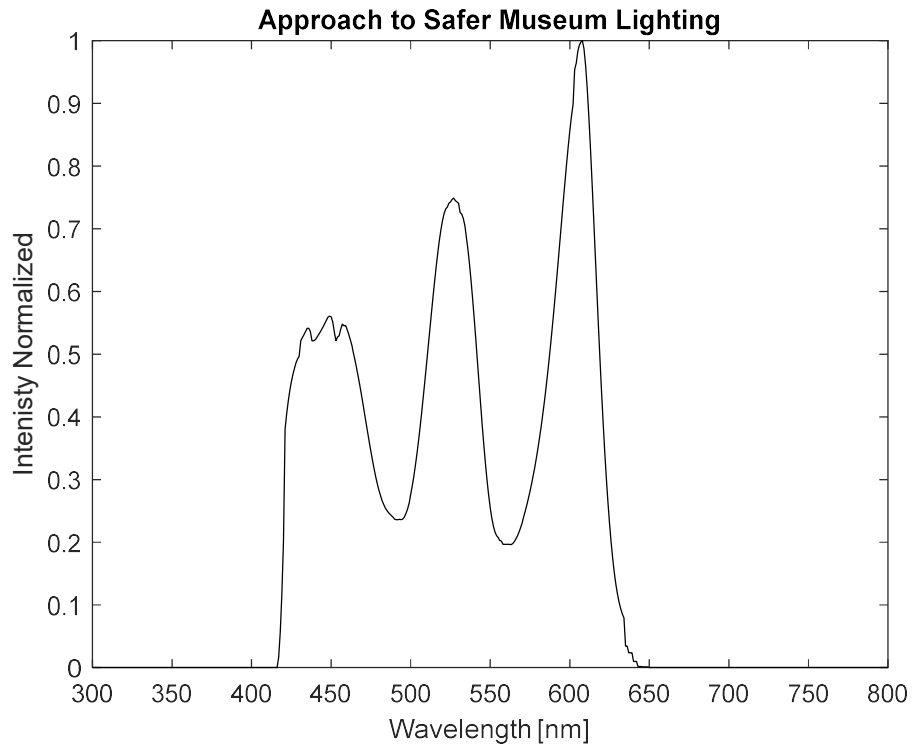


Fig. 2.12 Mark 3 SPD target

Table 2.2 Characteristic of Mark 3 SPD.

Mark 3	L/W efficiency	CIE 13.3 CRI	CRI (U*V*W)/OMD Basis	CRI (U*V*W/OMD basis)	CRI (E00)/OMD basis	CRI(E00 /Munsell basis)	CIE 13.3 CRI	Smallest R1-R14	CQS
Color model	232	83.2	96.4	95.4	97.9	93.7	83	R9:-49	80

**Table 2.3** Perceptual attributes of color result from Mark 3 SPD.

Filter Sample size	Brightness/Darkness	Color rendering	Perception of details	Overall satisfaction
Mark 3	99%	75%	72%	65%

### 2.3.2 SPD requirement for Plant Growth's McCree

The second SPD is taken from the publication: "Tunable multiple-LEDs combination spectrum for plants based on McCree PAR spectrum" by Latifa Bachouch <sup>(4)</sup>. The McCree photosynthesis action plants SPD was created in 1970<sup>(2,5)</sup>. However, it has been used nowadays to provide the optimal lighting conditions needed to produce fresh fruits and vegetables. In addition, it also reduces the pesticides and improves the efficiency of lamp producing light only in the wavelength range beneficial to the plants.

This SPD represents the action spectra, absorptance, spectral quantum yield of CO<sub>2</sub> uptake for the leaves of 22 species of crop plants, over the wavelength range of 350 to 750nm. The factors considered are the temperature, CO<sub>2</sub> concentration, flux of supplementary white radiation, leaf orientation, species factors, variety, age of leaf, and growth condition. Figure 2.13 shows the optimized McCree SPD <sup>(4)</sup>.

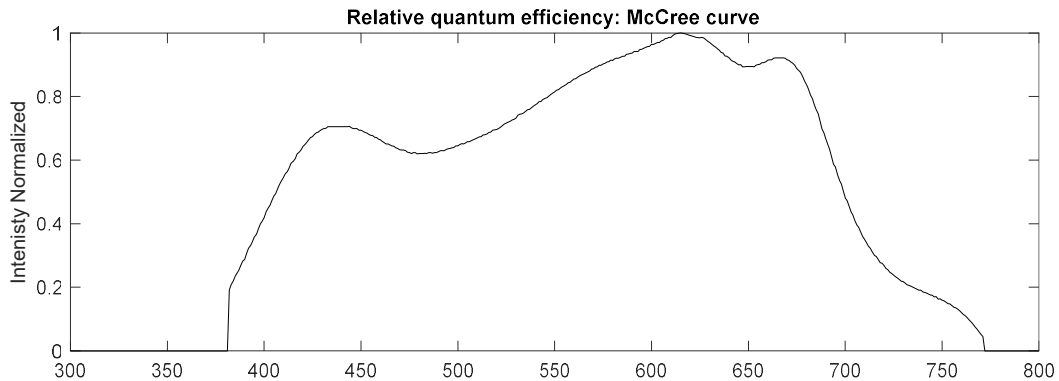


**Fig. 2.13** The Action spectrum, absorptance and quantum Yield of photosynthesis in crops plants

### 2.3.3 SPD requirement for the plant growth absorption

The widely used Photosynthesis Action Spectrum (PAS) is shown in Figure 2.14. It has been cited in many publications as “Plant Growth Absorption Spectrum Mimicking Light Sources” by Jwo-Huei Jou <sup>8</sup>. This desirable SPD emits light that covers three pigments. The main requirement for plants’ photosynthesis is the photosynthesis-action chlorophyll-a; however, the plant growth needs chlorophyll-b to assist the light absorption for chlorophyll-a, and the carotenoids to also assist the light absorption and further release any excessive photonic energy that might damage the chlorophyll-a and the chlorophyll-b pigments.

The photosynthetic action spectrum needed may vary with different plants and/or with the variations in growing roots, stems, leaves, and fruits in different seasons and/or at different times diurnally. As a result, the ideal lighting device should also possess a high degree of design freedom in spectrum-tailoring so that the resulting spectrum can better match what is needed by the chlorophyll-a, the chlorophyll-b, and the carotenoids, either individually or collectively.



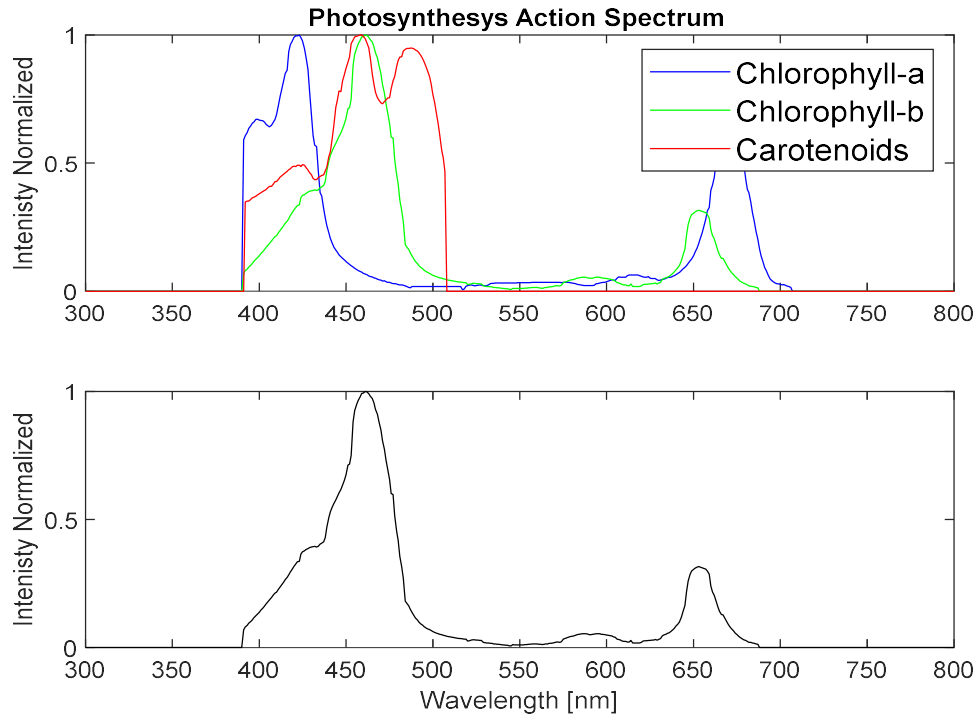


*Fig. 2.14 The upper subplot shows the absorption spectra of the chlorophylls a, and b; and the carotenoid pigments. The lower subplot shows the photosynthetic action spectrum.*

Then, a light source that accomplish those different requirements seen in 2.3 must be built. A single cathodoluminescent phosphor lamp can produce a fitted spectrum. It could be created by mixing the right proportion of the right phosphor materials. There are several monochromatic spectra since there are many color phosphors powder that can be selected. There are three popular techniques for mixing phosphor materials<sup>[38]</sup>; superimposed-layer screen, mixed-phosphor screen, and onionskin phosphor screen. The techniques are shown in Figure 2.15.

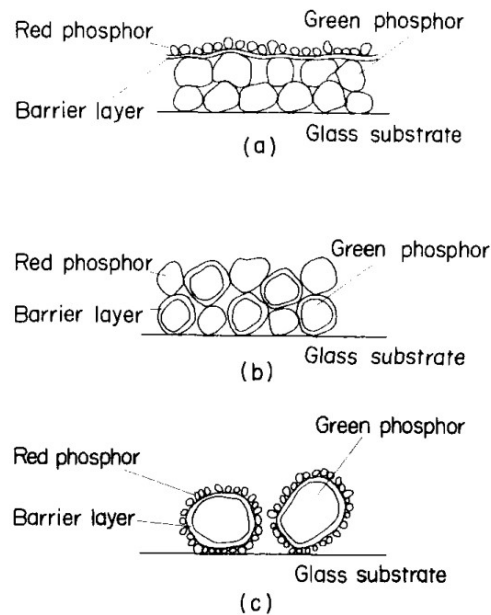


*Fig 2.15. Schematic examples of some idealized phosphor screens: (a) superimposed-layer screen; (b) mixed-phosphor screen; (c) onionskin phosphor screen.*

This idea has the advantage of using one excitation source. However, the technique requires a lot of effort since the same current density is applied to all the phosphor materials that have different properties. For example, the efficiency in terms of photon production, if one of the phosphors exceeds the others, this spectrum will dominate the rest since we were applying the same current density. Then, many material characteristics should be considered in the mixing, not only the SPD. Another main disadvantage is that once the color output is created. The structure does not allow any modification or tuning. This disadvantage can be considerable since the light sources suffer damage under excitation exposition. It can also be seen in the single-color white LEDs. The blue light excites the yellow photoluminescent materials and creates a broader spectrum, but it also damages the photoluminescent material, and after some time, the LED's output color gets bluish. In that sense, it is better to have a

source that is composed of many individual QMLS. It will allow changes in single light sources that modify the output colors. The main disadvantage is the increment of excitation sources and the selection of the excitation parameters.

## 2.4 Computational Model for the SPD

This subsection gives a mathematical and computational description of the problem of finding the single QMLS variables that when combined can closely match a desired SPD. It also explains how to solve the problem using the genetic algorithms (GA).

The GA model optimizes the variables of single QMLSs to obtain an SPD. These SPD are then combined to mimic a desired SPD. The GA model is designed with two different criteria; In the first one, the SPD of a QMLSs is given by SPD data collected, and this option is called Real QMLS. The second option is called Ideal QMLS, which considers the blackbody radiation equation to generate the SPD of the QMLS.

### 2.4.1 Mathematical models

The mathematical model presents the variables and the considerations to approach and solve the problem. The model is divided into the Ideal QMLS and the Real QMLS.

#### 2.4.1.1 Mathematical model for the SPD of QMLS

Ideal QMLS: This model assumes that the blackbody radiation equation produces the SPD of the a single QMLS. This consideration ensures that the model optimizes the three QMLS variables; however, these variables could simulate a lamp that may not be possible to fabricate. The GA

model obtains the individual values for the variables of the peak wavelength, the peak power, and the spectral width given by equation 19 shown below <sup>(11,12,13,14,15)</sup>:

$$SPD_{Ideal}(\lambda, Peak_w, Peak_p, Spectral_w) = \frac{Peak_p * \left( \exp\left(-\left(\frac{\lambda - Peak_w}{Spectral_w}\right)^2\right) + 2 \left( \exp\left(-\left(\frac{\lambda - Peak_w}{Spectral_w}\right)^2\right) \right)^5 \right)}{3} \quad \text{equation 19}$$

Where the  $Peak_p$  is the peak power, the  $Peak_w$  is the peak wavelength, and the  $Spectral_w$  is the spectral wavelength range <sup>(15)</sup>.

Real QMLS: This model assumes that the SPD results from the QMLS is given by the data collected. This consideration ensures that the model optimizes for the peak power variables or for the intensities of the SPD results from QMLSs <sup>(44)</sup>.

$$SPD_{Real}(Peak_p) = Peak_p * QMLS(\lambda_j) \quad j=1, \dots, k \quad \text{equation 20}$$

Where  $Peak_p$  is the intensity coefficient or the peak power,  $QMLS(\lambda_j)$  is the spectral distribution of the Quasi-monochromatic light source, and represents the data collected on sections 2.1 and 2.2, and k is defined as the number of wavelength data points collected in a given spectrum.

#### 2.4.1.2 The mathematical model for the fitted spectrum

Ideal QMLS: In this GA model, the fitted spectrum is defined by a group of Ideal QMLSs that their combined spectrum generate a desired SPD; it is a sum produced by equation 21.

$$S_f = \sum_{i=1}^n SPD_{Ideal}(\lambda, Peak_{w_i}, Peak_{p_i}, Spectral_{w_i}) \quad \text{equation 21}$$

$S_f$  is the fitted spectrum,  $n$  is the number of QMLSs,  $\lambda, Peak_{w_i}, Peak_{p_i}, Spectral_{w_i}$  are the fitting coefficients of the  $i$ th QMLSs,  $SPD_{ideal}$  is the ideal spectral distribution of the  $i$ th QMLS.

Real QMLS: In this GA model, the fitted spectrum is defined by a group of Real QMLSs that their combined spectrum offers us an approximate match to the desired SPD; and it is given by equation 22.

$$S_f = \sum_{i=1}^n SPD(\lambda_j, Peak_{p_i}) \quad \text{equation 22}$$

$S_f$  is the fitted spectrum,  $n$  is the number of selected QMLSs,  $Peak_p$  is the fitting coefficient of the  $i$ th QMLS,  $SPD(\lambda_j)$  is the spectral distribution of the  $i$ th QMLS.

Solving for the  $S_f$  with equations 21 and 22 generate an overdetermined matrix for the solution that has no exact solution in the classical sense <sup>(44)</sup>.

#### 2.4.2 Genetics algorithms model for the fitted Spectrum

Considering an overdetermined solution to the problem previously explained, a GA model is created to obtain the fitting coefficients for each QMLS such that when they are combined, generate artificial light source's SPD that meet the desired SPD requirement. The problem and solution are represented in a biological computational GA model.

##### 2.4.2.1 Chromosomic problem representation

The fitting coefficients for a single QMLS is represented here by genes. Multiple genes will represent a chromosome or, in our case, a possible fitted spectrum.

Real QMLS: Each gene is a value that represent the possible peak power or the intensity for the QMLS. The value is a floating-point number between 0 to 1. The value of 0 indicates no light in generated by the QMLS at hand, and the value of 1 indicates the maximum light intensity

allowed by that QMLS. Figure 2.16 shows an example of the GA model for the genes in the SPD; and Figure 2.17 shows some examples of the possible fitted spectrum variables that can produce an SPD by the combination of the genes described previously.

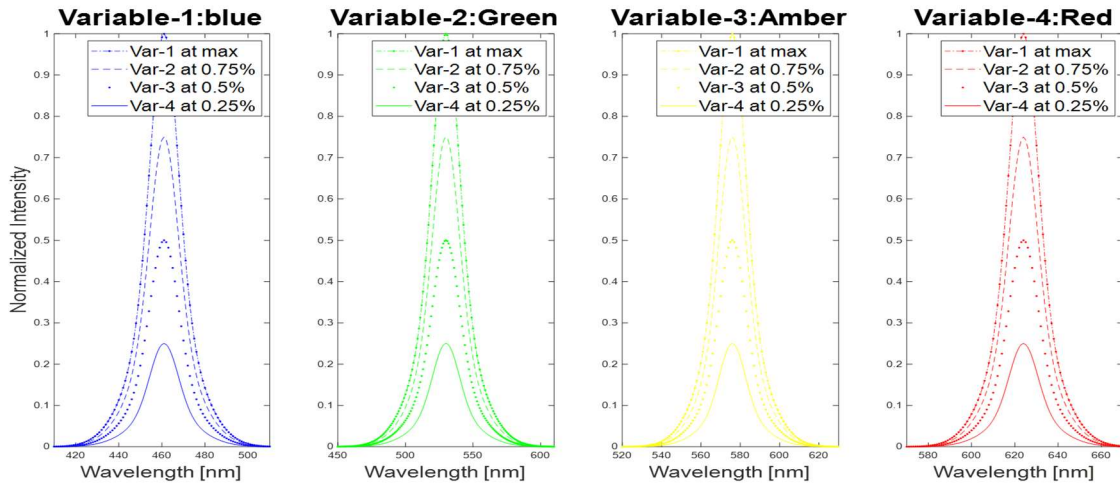


Fig. 2.16 Four QMLS with genes values of 1, 0.75, 0.5 and 0.25 of their maximum intensities normalized.

As an example of the representation, Figure 2.16 shows four QMLSs with their peaks at the colors of blue, green, amber and red. Where the SPD of an QMLS is modified by the gene values of 1, 0.75, 0.5, and 0.25. Figure 2.16 also shows the variation of wavelength-dependent intensity values as a result of this representation.

Then a fitted spectrum is given by the combination of those QMLSs as the chromosome is defined as the combination of genes. As an example, the chromosome data in figure 2.17 is plotted in figure 2.18, which shows the SPD profiles of those chromosome representations.

Chromosome 1	0.75	0.25	1	0.5
Chromosome 2	1	0.5	0.75	0.25
Chromosome 3	0.25	0.75	1	0.5
Chromosome 4	0.5	1	0.25	0.75

Fig. 2.17 Chromosomes: Each gene modifies the intensity of a single QMLS.

Figure 2.18 shows four possible fitted spectra or chromosomes created by the combination of the SPDs or the genes previously given and shown in Figure 2.16. Figure 2.17 shows the expected intensity profile result of the SPD of the chromosomes generated. The right subplots show the fitted spectrum when the four QMLSs spectra on the left subplot are combined or, in other words, added up wavelength-wise.

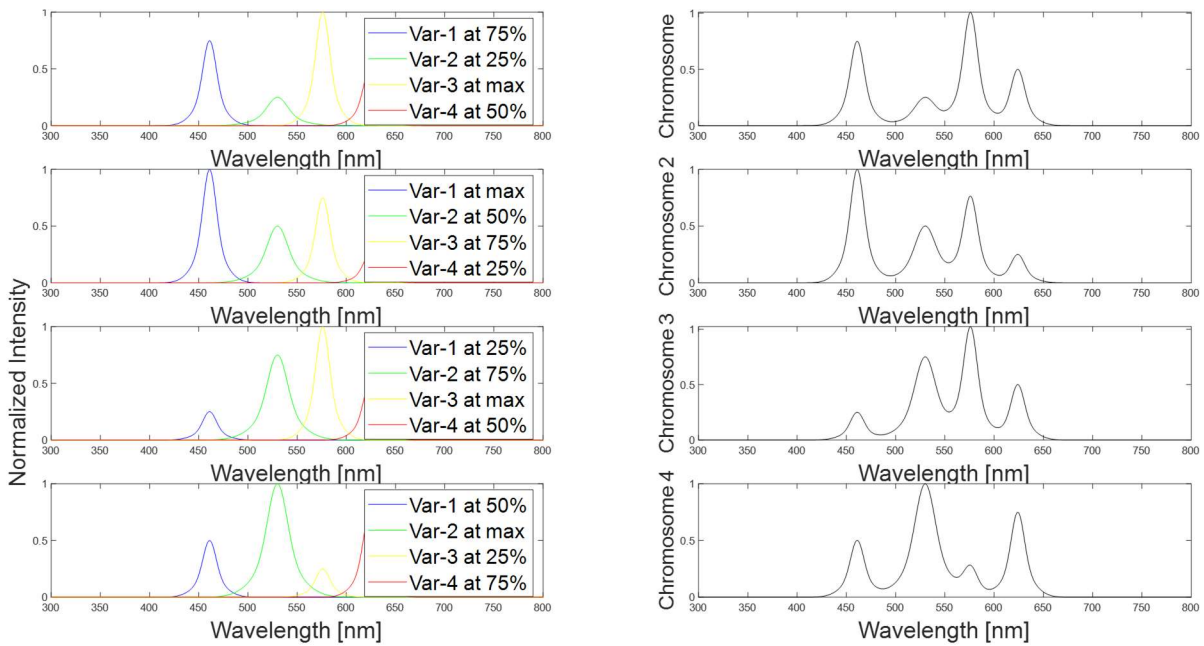


Fig. 2.18 Four chromosomes each composed by four SPDs.

Figure 2.18 shows four fitted curve options each generated by combining four QMLS modified by the four genes, the combination is generated by the superposition of the each single SPD using the additive color mixing.

#### 2.4.2.2 Chromosomic evaluation

The chromosomes or the fitted spectrum created must be evaluated and ranked by an equation called the fitness function. The R-Squared is a function, or a metric used to evaluate the variation between two curves or, more precisely, evaluate the scattering of the data points around a fitted regression line. It is also called the coefficient of determination. Higher R-squared values represent smaller differences between the desirable SPD and the fitted SPD. In this work, the R-Square function provides how the new SPD curve fits the desired SPD and is used as the fitness function to guide the GA.

R-squared is calculated as 1-minus the proportion of the sum of squared error and the to the sum of squared regression, and the final value is given by equation 23 <sup>(44)</sup>.

$$R^2 = 1 - \frac{\sum_{i=0}^n (\widehat{S}_f - S_f)^2}{\sum_{i=0}^n (S_f - \overline{S}_f)^2} * 100\% \quad \text{equation 23}$$

Here,  $\widehat{S}_f$  is the desired SPD,  $\overline{S}_f$  is the mathematical expectation value of  $S_f$ . The larger the value of the correlation coefficient  $R^2$ , the higher the fitting precision is. When  $R^2 = 1$ , the fitted spectrum entirely coincides with the target spectrum.

Other fitness functions can be used as the criteria for evaluating possible QMLS combinations. MATLAB App also contains functions related to the color quality indexes such as the CRI and the CCT. Other publications compare the energy emitted by the source and the energy needed by a desirable SPD with different equations.

#### 2.4.2.2 GA model in MATLAB



This subsection shows how the MATLAB Global Optimization toolbox, specifically its GA function is used to obtain the local solutions. The GA function will iterate the following steps to optimize the QMLS coefficients to obtain an SPD that mimics the desired SPD.

*a) Initial Population*

The genetic algorithm begins by creating a matrix  $M_{mn}$ , in which each row represents a fitted spectrum, and the number of rows  $m$  is the number of fitted Spectra created. Every column in the matrix represents a fitting coefficient, and the number of columns  $n$  is the number of genes, or the fitting coefficients used. As an example, for the Real QMLS, see the following 4x4 Matrix called the Initial Population.

$$Initial\ Population = \begin{bmatrix} 0.60 & 0.46 & 0.32 & 0.18 \\ 0.39 & 0.42 & 0.78 & 0.72 \\ 0.92 & 0.46 & 0.47 & 0.47 \\ 0.00 & 0.77 & 0.04 & 0.15 \end{bmatrix}$$

*Fig. 2.19 Matrix of four possible solutions with four QMLSs*

In the case of a real QMLS, each value represents the peak power or the intensities for each QMLS. The constrained parameters give the maximum and the minimum values in the GA function. The initial population matrix for the peak power shown in Figure 2.19 is created by a matrix with random values from 0 to 1. An element with a value of 0 represents that light is off, and the value of 1 represents the maximum light given by the QMLS.

*b) Creating the Next Generation*

The next generation is created using the evaluation, selection, crossover, and mutation steps. The performance of the current generation is ranked using the fitness function as shown

in figure 2.20. The ranking represents the quality of the solution providing the information used in the selection criteria, which serves to preserve the best chromosomes and share their genes or variables with the next generation. The selection can be specified on MATLAB by selecting the parents in the SelectionFcn option. The new generation starts by evaluating the chromosomes, as in Figure 2.20, which shows the ranking of the chromosomes for each solution. Figure 2.21 shows the new matrix after being sorted by the ranking.

$$Initial\ Population = \begin{bmatrix} 0.60 & 0.46 & 0.32 & 0.18 \\ 0.39 & 0.42 & 0.78 & 0.72 \\ 0.92 & 0.46 & 0.47 & 0.47 \\ 0.00 & 0.77 & 0.04 & 0.15 \end{bmatrix} \begin{matrix} ranking = 3 \\ ranking = 2 \\ ranking = 1 \\ ranking = 4 \end{matrix}$$

*Fig. 2.20: Ranking for each chromosome after the fitness evaluation.*

$$Initial\ Population\ after\ ranking = \begin{bmatrix} 0.92 & 0.46 & 0.47 & 0.47 \\ 0.39 & 0.42 & 0.78 & 0.72 \\ 0.60 & 0.46 & 0.32 & 0.18 \\ 0.00 & 0.77 & 0.04 & 0.15 \end{bmatrix}$$

*Fig. 2.21: Matrix obtained after sorting the initial population by the ranking.*

In the case of real QMLS, the rows of the current population are ranked by using R square metric, and the value represents how much the created SPD mimics the desired SPD. A new matrix is created then by sorting the current population by the R-square ranking.

- *Selection*

The selection process for the new generation is based on the information provided by the fitness function. The selection of the best individuals based on their quality is executed; and the individual or the chromosome with a higher quality or fitness has a higher probability of

being selected, preserving the information in their gene for the next generation. In the example given, after the four chromosomes are ranked, and the selection process preserves the two chromosomes that have better ranking and remove the other two chromosomes.

$$Selection = \begin{bmatrix} 0.92 & 0.46 & 0.47 & 0.47 \\ 0.39 & 0.42 & 0.78 & 0.72 \\ \del{0.60} & \del{0.46} & \del{0.32} & \del{0.18} \\ \del{0.00} & \del{0.77} & \del{0.04} & \del{0.15} \end{bmatrix} \begin{matrix} Preserved \\ Discarded \end{matrix}$$

Fig. 2.22: Description of the New matrix after the selection process.

Figure 2.22 shows the new ranked matrix by denoting the chromosomes that are selected and to be discarded. The discarded chromosomes do not produce SPD. Every row that is preserved is called a parent for the next generation.

- *Crossover Children*

The GA model creates what is called a crossover child by combining a pair of parents in the current population. For every pair of parents, the crossover takes place by selecting a random point or gene index in the chromosome and exchanging the genes before and after that point from its distinct parents. The resulting chromosomes are called offspring or the crossover children. The Crossover-Fraction option in MATLAB specifies the fraction of each population, other than what is called the elite children, that are made up of the crossover children. An illustration of the crossover point is shown in Figure 2.23.

$$Matrix\ after\ Selection = \begin{bmatrix} 0.92 & 0.46 & 0.47 & 0.47 \\ 0.39 & 0.42 & 0.78 & 0.72 \end{bmatrix} Preserved\ Information$$

Fig. 2.23 Matrix after the selection process.

$$\text{After Breeding} = \begin{bmatrix} 0.92 & 0.46 & 0.47 & 0.47 \\ 0.39 & 0.42 & 0.78 & 0.72 \\ 0.92 & 0.46 & 0.78 & 0.72 \\ 0.39 & 0.42 & 0.47 & 0.47 \end{bmatrix} \begin{matrix} \text{Parents} \\ \text{Offspring} \end{matrix}$$

Fig. 2.24 Matrix after the crossover process.

In the example for real QMLS shown in Figure 2.24, the new matrix is created after the crossover process provides two new SPD solutions from the coefficients of the parents which have already generated the best solutions in the previous matrix.

- *Mutation of the Children*

The algorithm creates mutation in the crossover children by randomly changing the random genes of the individual parents. In MATLAB, the algorithm adds a random vector from a Gaussian distribution to the parent by default. The mutation is deliberate to stop the falling of all population solutions into a local optimum of the solved problem. For each offspring, some genes are selected to change their value. An illustration of the mutation is shown in Figure 2.25.

$$\text{After Mutation} = \begin{bmatrix} 0.92 & 0.46 & 0.47 & 0.47 \\ 0.39 & 0.42 & 0.78 & 0.72 \\ 0.92 & 0.46 & 0.64 & 0.72 \\ 0.20 & 0.42 & 0.47 & 0.47 \end{bmatrix}$$

Fig. 2.25 Matrix after mutation.

Figure 2.25 shows the new matrix formed by the mutation step. The new matrix has two new elements with mutated values 0.64 in the 3er row and 0.20 in the 4er row that add two new intensities to the pool. Those values also follow the constrained parameters used for the initial population which in this case is the range between 0 and 1.

### c) Stopping criteria

The number of iterations in the optimization process depends on a solver's *stopping criteria*. These criteria include several *tolerances* parameters that can be set. Generally, the tolerance is a threshold that stops the iterations of a solver if it is crossed. In MATLAB, the GA has multiple options to determine when to stop, MaxGenerations, MaxTime, FitnessLimit, MaxStallGenerations, MaxStallTime, FunctionTolerance, and ConstraintTolerance. The default values for each option can be defined by running the command: `opts = optimoptions('ga')`.

# Chapter 3

## Results and Discussion

This chapter exhibits and analyses the results of the GA model described in section 2.4.

The results and analysis are divided into three sections as follows:

- Section 3.1: The GA model obtained the fitting coefficients for Real QMLS that combined a set of QMLS to fit a desired SPD. The SPD of the QMLS used the real data collected in the Vacuum Microelectronics Laboratory.
- Section 3.2: The fitting coefficients obtained by the GA model in section 3.1 are implemented in a real lamp to produce the expected SPDs. The new SPDs are collected and compared with the simulated values.
- Section 3.3: The GA model optimized the fitting coefficients for the Ideal QMLS that produce a new SPD that mimics the desired SPD.

Each section is divided into three subsections that optimized the fitting coefficients for three applications: The Preserving Museum Artifacts, the Plant Growth's McCree, and the Photosynthesis Active Spectrum.

### 3.1 Simulation Results Using Real QMLS

This section focuses on the results obtained by the GA model for Real QMLSs. The model obtains the peak power, or the intensities of the light sources explained in sections 2.1 and 2.2. The model optimized the fitting coefficients for each QMLS and then combined their spectra to

emulate the targets profiles explained in section 2.3. The light sources were divided and grouped into four categories as follows:

- **CL:** The first group is a combination of the three cathodoluminescent phosphors, SPDs of which were described in section 2.2.

The other three groups are composed of the LEDs sources described in section 2.1 and grouped as follows:

- **BGAR:** The new SPD considers LEDs with the colors of blue (B), green (G), amber (A), and red (R).
- **BGR:** The new SPD considers LEDs with the colors of blue, green, and red.
- **BAR:** The new SPD considers LEDs with the colors of blue, amber, and red.

The bound for fitting coefficients of the Real QMLSs considers a maximum of four times and a minimum of 0 times of the normalized SPD’s peak obtained at the excitation current of 350 mA.

The simulation results are shown and compared in Tables 3.1, Table 3.2, and Table 3.3, and the new SPDs are plotted in Figure 3.1, Figure 3.2, and Figure 3.3.

### 3.1.1 Simulation results for Preserving Museum Artifacts using Real QMLSs

The individual intensity results fitted to the SPD for the preserving museum artifacts are shown in Table 3.1 and plotted in Figure 3.1

**Table 3.1:** Fitting coefficient results for Real QMLS to fit the Preserving Museum Artifact’s SPD

QMLS	Blue	Green	Amber	Red	R-square
CL-BGR	0.1	0.64	-	1.72	<b>0.015</b>

<b>BGR</b>	0.1	1.22	-	1.99	<b>0.015</b>
<b>BAR</b>	0.1	-	3.2	1.92	<b>0.05</b>
<b>BGAR</b>	1.18	0.95	1.77	0.1	<b>0.1</b>

Table 3.1 shows that the optimized groups of QMLS generate fitted spectra with a low R-square value.

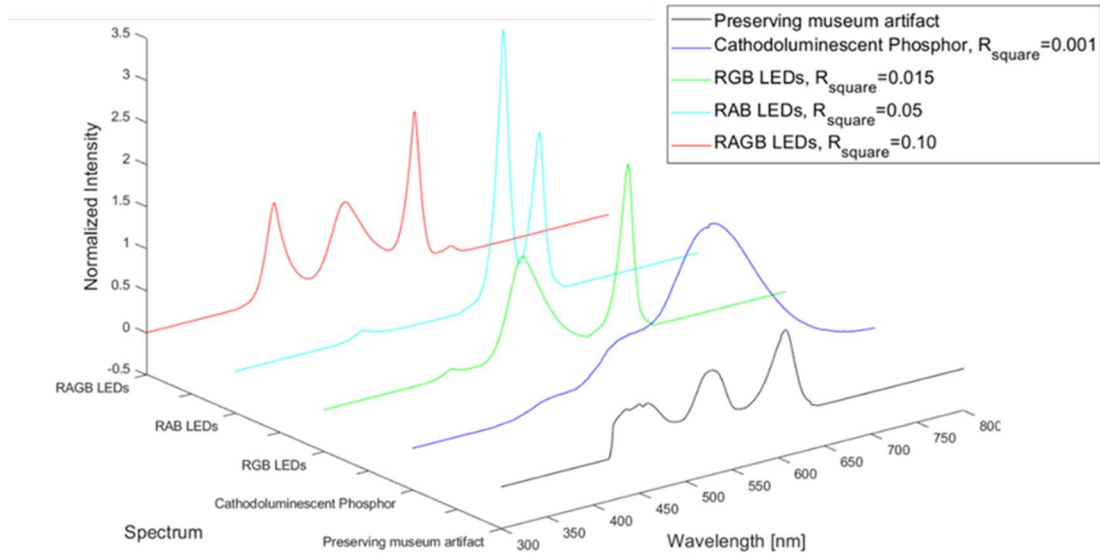


*Fig. 3.1 SPD simulation results for fitting the preserving museum artifact's SPD*

Figure 3.1 shows a 3D plot with the optimized fitted spectra obtained by the GA model for the group of QMLS described previously and for the purpose of preserving museum artifacts. One of the reasons for the low R-square values is because the desired SPD has the particularity of two narrow bands that the QMLSs must fit, and as a consequence, the CL shows the worst performance since they have the wider spectra. In the LEDs groups, the blue peak does not produce any improvement due to its peak being out of the desired spectrum.



### 3.1.2. Simulation results for the Plant Growth's McCree using Real QMLSs

The GA model's fitting coefficients data for the plant growth's McCree SPD are shown in Table 3.2 and plotted in Figure 3.2.

**Table 3.2:** Fitting coefficient results for Real QMLS to fit the Plant Growth's McCree's SPD

QMLS	Blue	Green	Amber	Red	R-square
<b>CL-BGR</b>	0.76	1.16	-	0.72	<b>0.186</b>
<b>BGR</b>	1.92	2.12	-	4	<b>0.156</b>
<b>BAR</b>	2.33	-	4	4	<b>0.179</b>
<b>BGAR</b>	1.58	1.57	2.85	3.18	<b>0.260</b>

Table 3.2 shows that CL lamp has a better performance when considering the same number of QMLSs. It also shows that the amber and red intensity variables reach their upper bound when considering the BGR-LED and BAR-LED groups.

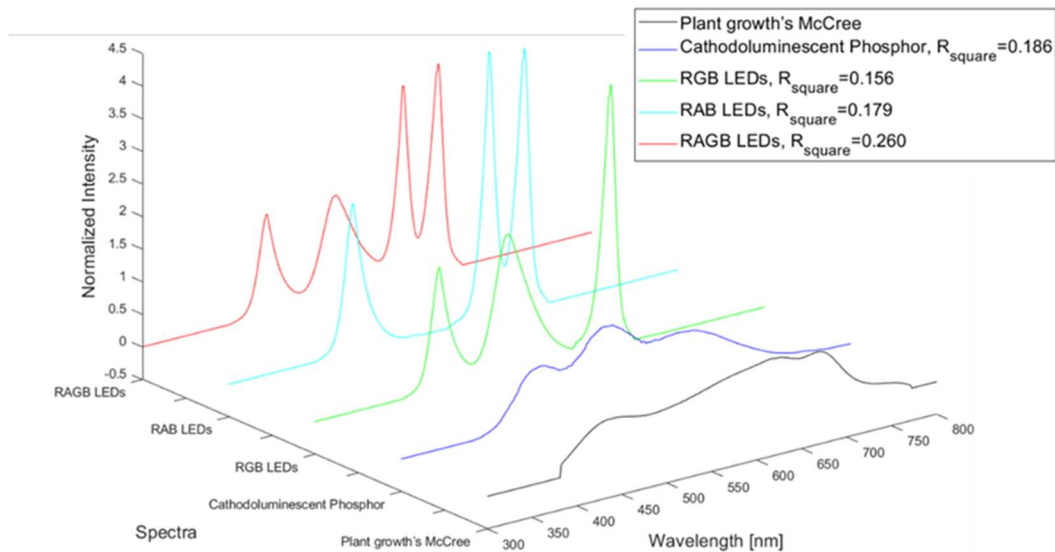


*Fig. 3.2 SPD simulation results after fitting to the plant growth's McCree SPD.*

Figure 3.2 and the R-Square results in table 3.2 show that the width of the desirable SPD is a critical factor. The CL QMLSs produce a better fit here using the same number of QMLS because of their wider spectra. The best performance, however, is exhibited using four LEDs,

which is explained by the wider wavelength range covered using four QMLSs and the option to manage an extra QMLS intensity separately.

In addition, the amber and red intensities reached their upper bound, and it is due to the fact that the GA model can increase the spectral width only by increasing the peak of the QMLSs. This dependency can be problematic since some requirements take into account the energy absorbed by the target or the energy emitted by the source.

### 3.1.3. Simulation results for the photosynthesis active spectrum’s SPD

The fitted individual intensity results for the photosynthesis active spectrum’s SPD are shown in Table 3.3 and plotted in Figure 3.3.

**Table 3.3:** Fitting coefficient results for Real QMLS to fit the Photosynthesis Active Spectrum’s SPD

QMLSs	Blue	Green	Amber	Red	R-square
CL	1.72	0.1	-	0.62	0.55
BGR	1.17	0.66	-	4	0.17
BAR	1.75	-	0.1	4	0.16
BGAR	1.16	0.64	0.1	4	0.177

Table 3.3 shows a much better performance obtained from the CL lamp. It also shows a non-considerable difference between the groups of 3 and 4 LEDs in terms of R-Square results.

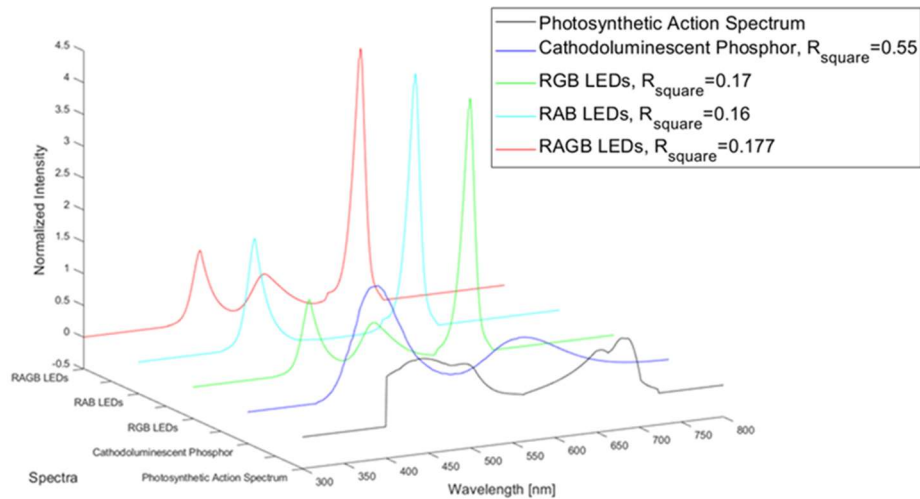


Fig. 3.3: SPD simulation results after fitting to the Photosynthesis Action Spectrum's SPD.

Figure 3.3 shows that the width of the desirable SPD peaks is a critical requirement for the fitted spectrum. CL QMLS produce the best fitting to the PAS since they have wider FWHMs than the LEDs. It also shows that the Red LEDs do not improve the lamp's performance since its peak is out of desired range. The Red LED reaches the maximum bound because the GA model tries to increase its FWHM by increasing its peak power.

### 3.2 Experimental results

This section shows the experimental results of a group of LEDs excited to obtain the intensities simulated by the GA model shown in section 3.1. The SPD, the current, the voltage, the luminous flux, and the luminance values are measured, and the data is collected and processed.

The data analysis of the SPD considered all the points collected by the USB4000 spectrometer in the desired SPD wavelength range. Furthermore, The LED intensities consider a

maximum of around 350 mA as the current excitation; and extra luminous flux requirement can be reached by adding more LEDs sources. This situation does not imply a higher cost in terms of the excitation sources since the voltages will be the same. However, the voltage sources should provide enough current to obtain the desired intensity levels.

### 3.2.1 Experimental results for Preserving Museum artifacts

In the following experiments, a set of LEDs are excited and combined to fit the ideal SPD for Preserving Museum Artifacts simulated in section 3.1.1. The individual excitation and the response can be found in Table 3.4, Table 3.5, and Table 3.6. The R-Square values show the agreement between the simulation and the experimental values. Figure 3.4 shows the final SPDs obtained using the groups of LEDs.

**Table 3.4.** Excitation values and the R-square experimental results using the BGAR lamp.

LED	Blue	Green	Amber	Red	BGAR Lamp
Current [mA]	172	200	293	5.1	670
Voltage [V]	2.6	3.3	2.15	1.6	-
Flux [lm]	145.2	39.54	42.56	0.8	227
R Square	0.9903	0.9645	0.9983	0.9782	0.9797

**Table 3.5:** Excitation values and the R-square experimental results using the BGR lamp.

LED	Blue	Green	Red	BGR Lamp
Current [mA]	15.45	458	147.7	616
Voltage [V]	2.5	3.6	2	-
Flux [lm]	16	68	22	106
R Square	0.8856	0.9993	0.9964	0.9969

**Table 3.6:** Excitation values and the R-square experimental results using the BAR lamp.

LED	Blue	Amber	Red	BAR Lamp
Current [mA]	10.3	293	56.1	359.4
Voltage [V]	2.5	2.15	1.7	-

<b>Flux [lm]</b>	9	47	8.9	64.9
<b>R Square</b>	0.8603	0.9992	0.9857	0.9947

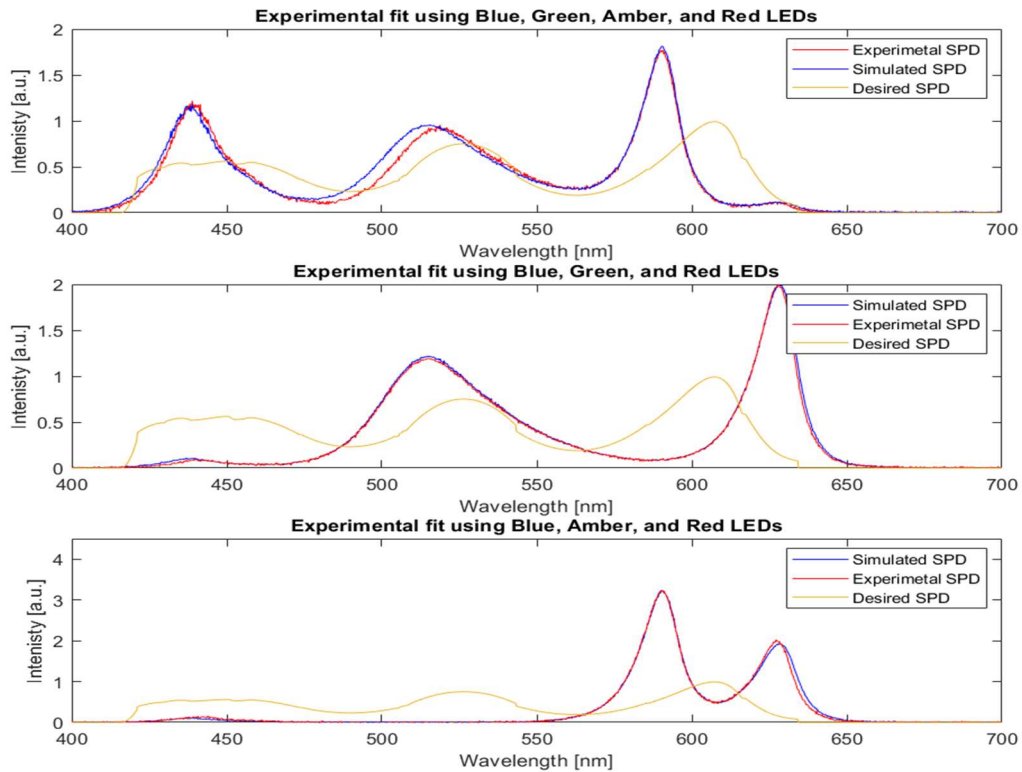


Fig. 3.4 Experimental SPD profiles using LEDs for Preserving Museum artifacts.

### 3.2.2 Experimental results for the Plant Growth's McCree by using Real QMLs

In the following experiments, a set of LEDs are excited and combined to fit the Plant Growth's McCree SPD simulated in section 3.1.2. The individual excitation parameters and the corresponding response values can be found in Table 3.7, Table 3.8, and Table 3.9. Figure 3.5 shows the fitted spectrum obtained using LEDs.

**Table 3.7:** Excitation values and the R-square experimental results using the BGAR lamp.

<b>LED</b>	<b>Blue</b>	<b>Green</b>	<b>Amber</b>	<b>Red</b>	<b>Lamp</b>
<b>Current [mA]</b>	157	261.6	293	102.8	670
<b>Voltage [V]</b>	2.6	3.4	2.15	1.9	-
<b>Flux [lm]</b>	134	47.15	47	15.24	243.39

<b>R Square</b>	0.9890	0.9857	0.9988	0.9918	0.9892
-----------------	--------	--------	--------	--------	--------

**Table 3.8:** Excitation values and the R-square experimental results using the BGR lamp.

<b>LED</b>	<b>Blue</b>	<b>Green</b>	<b>Red</b>	<b>Lamp</b>
<b>Current [mA]</b>	283	458	208	949
<b>Voltage [V]</b>	2.8	3.6	2.1	-
<b>Flux [lm]</b>	294	75	31.7	400.7
<b>R Square</b>	1.0000	0.9990	0.9992	0.9990

**Table 3.9:** Excitation values and the R-square experimental results using the BAR lamp.

<b>LED</b>	<b>Blue</b>	<b>Amber</b>	<b>Red</b>	<b>Lamp</b>
<b>Current [mA]</b>	144	293	86.4	523.4
<b>Voltage [C]</b>	2.6	2.15	1.9	
<b>Flux [lm]</b>	125	47.6	13	185.6
<b>R Square</b>	0.9907	0.9990	0.9915	0.9932

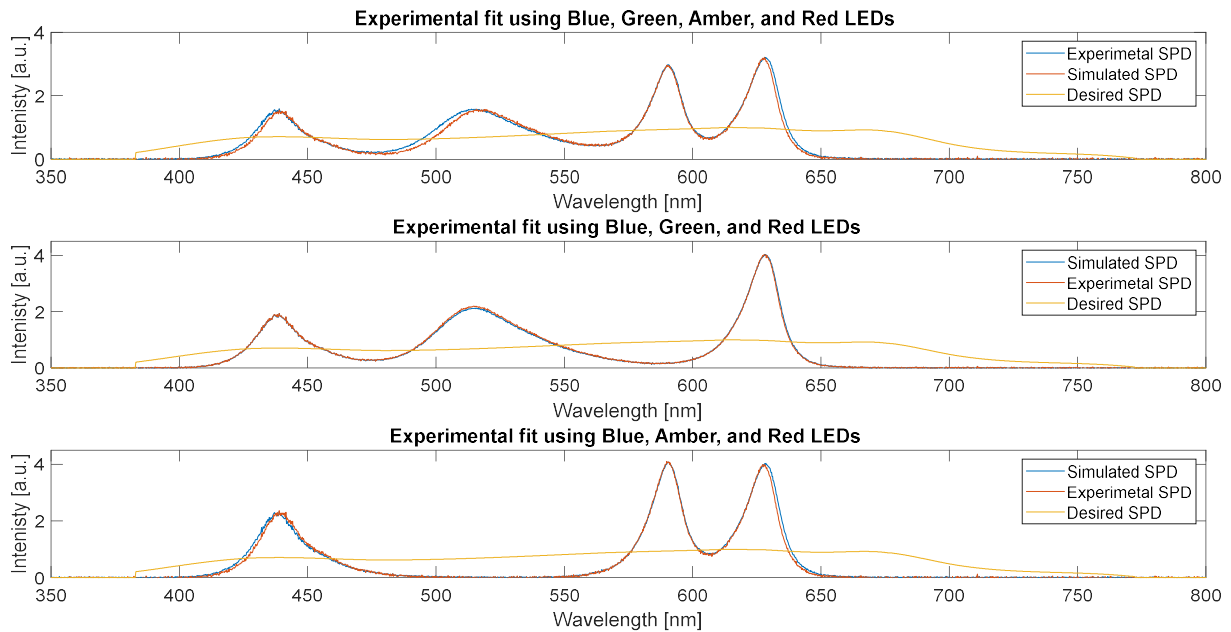


*Fig. 3.5 Experimental SPD profiles using LEDs to fit the Plant Growth's McCree.*

### 3.2.3 Experimental results for the Photosynthesis Active Spectrum

In the following experiment, a set of LEDs are excited and combined to fit the Photosynthesis Active Spectrum's SPD simulated in section 3.1.3. The individual excitation values and the corresponding R-square response for each LED source can be found in Table 3.10, Table 3.11, and Table 3.12. Figure 3.6 shows the final SPD plot obtained using LEDs.

**Table 3.10:** Excitation values and the R-square experimental results using the BGAR lamp.

LED	Blue	Green	Amber	Red	Lamp
Current [mA]	100	57.7	5	102.8	265.5
Voltage [V]	2.6	2.55(2.81)	1.9	1.9	-
Flux [lm]	89.56	14	1	15.24	119.8
R Square	0.9682	0.7899	0.2981	0.9916	0.9766

**Table 3.11:** Excitation values and the R-square experimental results using the BGR lamp.

LED	Blue	Green	Red	Lamp
Current [mA]	287	245	400	932
Voltage [V]	2.8	3.4()	2.2	-
Flux [lm]	216	45	48	309
R Square	0.9980	0.9858	0.9759	0.9744

**Table 3.12:** Excitation values and the R-square experimental results using the BAR lamp.

LED	Blue	Amber	Red	Lamp
Current [mA]	283	34.9	208	553
Voltage [V]	2.8	1.9	2.1	-
Flux [lm]	214	5	31.22	250.22
R Square	0.9989	0.9515	0.9992	0.9991

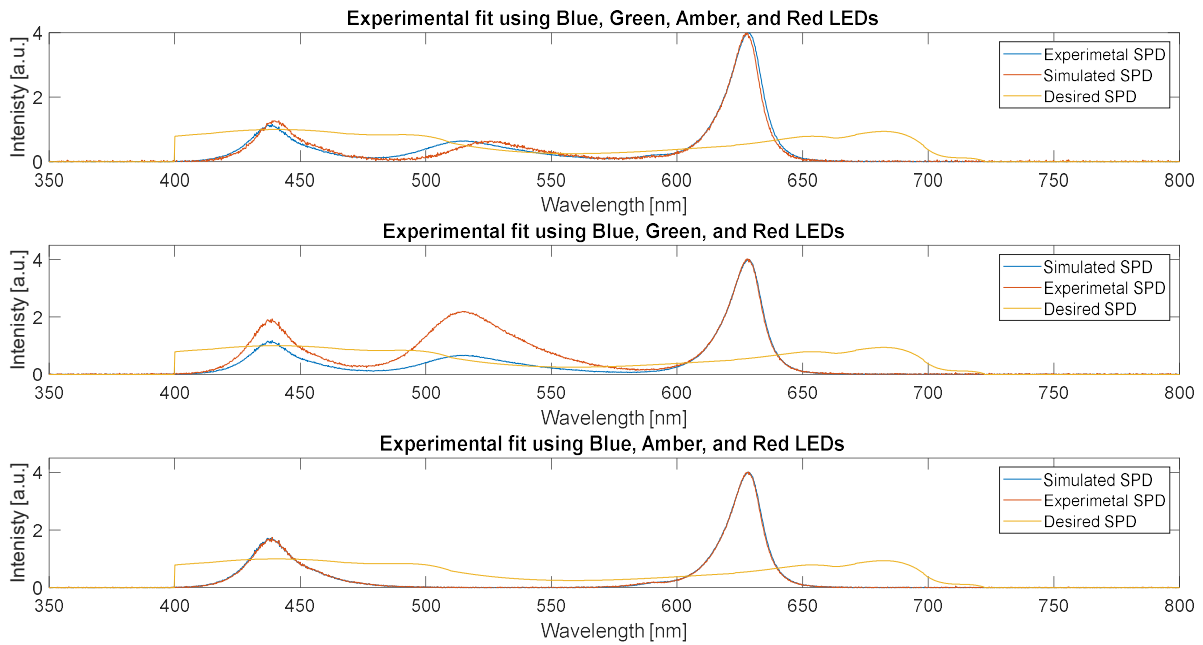


Fig. 3.6 Experimental fits to emulate the SPD of photosynthesis action spectrum using different groups of LEDs.

### 3.3 Simulation Results Using Ideal QMLSs

In this subsection, the GA model optimized the fitting coefficients for an ideal artificial light source based on QMLSs. The combination of each constituent QMLS with optimized coefficients produces a fitted spectrum that tries to match the desired SPDs described in section 2.3. The GA model outputs the fitting coefficients of the peak wavelength, the spectral width, and the peak power for a group of ideal QMLSs, SPD profiles of which are simulated by equation 19. The GA model evaluates a new SPD superimposing a group of one, two, three, and four ideal QMLSs. The new SPD can be implemented using either the CL or the LED sources.

The fitting coefficients for a GA model requires inputting the bounds, for which we have the following considerations:



- The bounds for the spectral width are between 10nm and 150nm, the maximum of 150nm can be obtained using a CL QMLS, and the minimum of 10nm can be obtained by using an LED.
- The bounds for the peak power have a maximum level that is 4 times the maximum normalized intensity of the desired SPD.
- The bounds for the peak wavelength are taken as 300 nm and 800 nm. A wide range of freedom for each QMLS increases the computational effort and time but may decrease the actual quality of the results. As a consequence, the simulation was further limited by a segment of this visible range of wavelengths for every QMLS. The range limits of these segments were selected by inspection of the desired SPD.

### 3.3.1. Simulation results for Preserving Museum Artifact using ideal QMLSs

In this subsection, the GA model optimized the fitting coefficients for the Ideal QMLSs that combined fit the SPD for preserving Museum Artifacts. The GA Model has three fitting coefficients; and the bounds for the wavelength peaks of different groups of QMLS are shown in Table 3.13. The criteria for the peak wavelength bounds are described below.

- In the case of only one QMLS, the bounds for the peak wavelength are restricted to the wavelength range between 500 nm and 550 nm. This additional restriction considers that this range of light reduces the damage compared to the red and the blue light; and increases the CRI response, which is one the most critical parameters for this application's desired SPD. Without this consideration, the GA model will tend to select

peaks around 400 nm or 600 nm since these values produce better fits in terms of the R-square function.

- In the case of four QMLSs, the bounds for the first peak wavelength were 400 nm and 500 nm. The bounds for the second peak wavelength were set to 500 nm and 600 nm. Likewise, the range for the third peak wavelength was chosen to be between 600 nm and 700 nm; but the last one was chosen to have a wider range between 400 nm and 700 nm adding more freedom to the system.

**Table 3.13:** Peak wavelength bounds used in the GA model for Preserving Museum Artifacts.

Number of QMLSs		Lower bound	Upper bound
1	QMLS 1	500	550
2	QMLS 1	400	550
	QMLS 2	550	700
3	QMLS 1	400	500
	QMLS 2	500	600
	QMLS 3	600	700
4	QMLS 1	400	500
	QMLS 2	500	600
	QMLS 3	600	700
	QMLS 4	400	700

The simulation results are shown and compared in Table 3.14 and are plotted in Figure 3.7. The MATLAB App also provides additional metrics of the CCT and the CRI indexes, on the top of the results. Those indexes are relevant to the selection of a lighting source for museum artifacts to display their true colors and details.

**Table 3.14:** Simulated parameters and results for preserving museum artifacts by using ideals QMLSs

# of QMLS		Peak W [nm]	Spectral W [nm]	Peak P [times]	R-Square	CCT	CRI
One	QMLS 1	526.2	20.8	1.95	0.127		73.7,46.22
Two	QMLS 1	481.9	173.3	0.7	0.533		55.7,65.9
	QMLS 2	605.1	20.0	1.21			
Three	QMLS 1	446.6	60	0.77	0.957		86, 65.9

	QMLS 2	526.9	38.6	0.87			
	QMLS 3	604.1	32.8	1			
Four	QMLS 1	464.4	28.7	0.32	0.995		81.19
	QMLS 2	438.1	40.2	0.53			
	QMLS 3	526.2	41.3	0.78			
	QMLS 4	604.1	31.1	1.01			

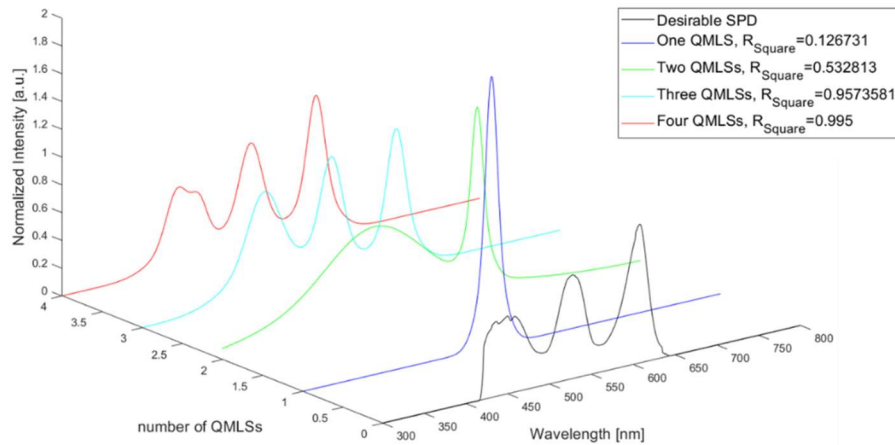


*Fig. 3.7 SPD results using different quantities of ideal QMLSs to fit to the SPD of Preserving Museum Artifacts.*

Table 3.14 and Figure 3.7 show that the R-square score is significantly higher using three or four QMLSs. The narrow spectral widths of the ideal QMLSs imply that the lamp should be constructed by using LED technology. The addition of another QMLS after three QMLSs is not significant enough, and considering the increment in the cost of additional voltage sources makes this effort worthless.

### 3.3.2. Simulation results for the Plant Growth's McCree's SPD by using ideal QMLS

In this subsection, the result of the GA model which optimized the fitting coefficients of the ideal QMLSs to reach a close fit to the Plant Growth's McCree SPD are evaluated. The GA Model has three fitting coefficients, and the bounds for the different groups of QMLSs' peak wavelengths are shown in Table 3.15. The criteria for the peak wavelength bounds are described below.

- The ranges were selected by equivalent distance: dividing the visible light spectrum by the number of QMLSs used for the new artificial light source.

**Table 3.15:** Peak wavelength bounds used in the GA model for the Plant Growth’s McCree’s SPD

Number of QMLSs	QMLS	Lower bounds	Upper bounds
1	QMLS 1	300	800
2	QMLS 1	300	550
	QMLS 2	550	800
3	QMLS 1	300	450
	QMLS 2	450	600
	QMLS 3	600	750
4	QMLS 1	300	700
	QMLS 2	300	450
	QMLS 3	450	550
	QMLS 4	550	800

The optimized fitting coefficients and R-Square results are shown in Table 3.16 and plotted in Figure 3.9.

**Table 3.16:** Simulated parameters results for the Plant Growth’s McCree’s SPD using ideal QMLSs

Number of QMLS		Peak W [nm]	Spectral W [nm]	Peak P [Times]	R-Square
One	QMLS 1	588.6	200	1.10	0.64
Two	QMLS 1	447.4	117.9	0.77	0.90
	QMLS 2	613.8	170.5	1.04	
Three	QMLS 1	442.8	106.0	0.78	0.976
	QMLS 2	592.1	157.7	0.98	
	QMLS 3	671.7	53.5	0.72	
Four	QMLS 1	630.6	124.6	0.68	0.995
	QMLS 2	437.6	94.4	0.60	
	QMLS 3	553.4	144.2	0.57	
	QMLS 4	676.9	46.2	0.34	

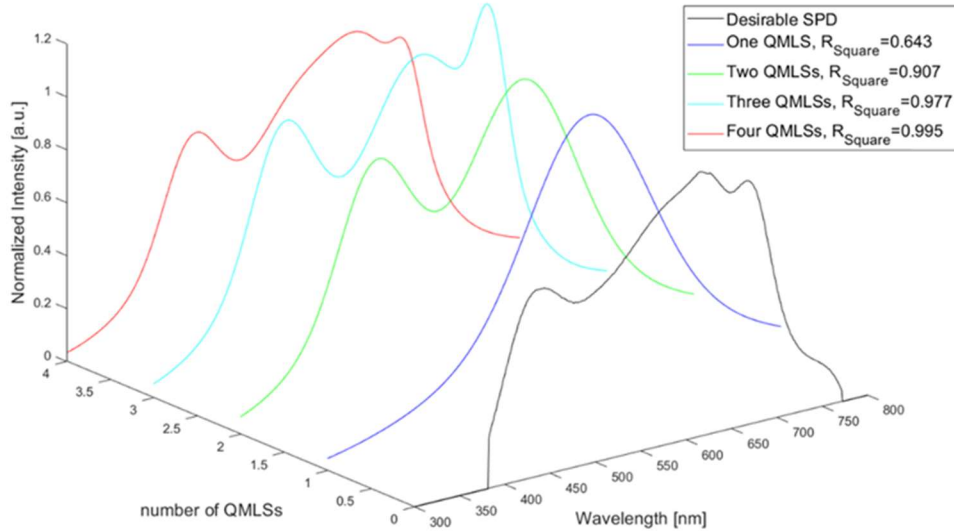


Fig. 3.9 SPD results using different quantities of ideal QMLSs to fit to the Plant Growth's McCree SPD.

The results are shown in Table 3.16 and Figure 3.9. The R-Square results are much better when using more than two QMLSs. However, the improvement may not be significant when considering additional QMLSs. The results also show that when using three QMLSs, the CL QMLSs can produce a better fit than LEDs, and it is due to the characteristic of CL's spectral width, which is wider than that LEDs.

### 3.3.3. Simulation results for the Photosynthesis Active Spectrum using ideal QMLS

In this subsection, the GA model optimized the fitting coefficients of the Ideal QMLSs that when combined simulates the Photosynthesis Action Spectrum. This GA Model has three fitting coefficients, and the peak wavelength bounds for the different groups of QMLSs are shown in Table 3.17. The criteria for the peak wavelength bounds were again the equivalent wavelength distance principle, that is: dividing the visible light spectrum by the number of QMLSs used to create the new simulated SPD.

**Table 3.17:** Peak wavelength bounds used in the GA model for the photosynthesis active spectrum's SPD

Number of QMLSs	QMLS	Lower bounds	Upper bounds
1	QMLS 1	300	800
2	QMLS 1	300	550
	QMLS 2	550	800
3	QMLS 1	300	450
	QMLS 2	450	600
	QMLS 3	600	750
4	QMLS 1	300	700
	QMLS 2	300	450
	QMLS 3	450	550
	QMLS 4	550	800

The fitted coefficient values and the R-Square are shown in Table 3.18 and plotted in Figure 3.10.

**Table 3.18:** Simulated parameters and the curve-fit results for the SPD of the photosynthesis action spectrum using ideal QMLSs.

Number of QMLSs		Peak W [nm]	Spectral W [nm]	Peak P [a.u.]	R-Square
One	QMLS 1	441.7	122.6	1.30	0.378
Two	QMLS 1	444.7	148.9	1.02	0.895
	QMLS 2	664.6	75.2	0.94	
Three	QMLS 1	445.2	145.9	1.02	0.904
	QMLS 2	600.0	43.1	0.37	
	QMLS 3	666.9	68.5	0.95	
Four	QMLS 1	421.0	118.7	0.78	0.971
	QMLS 2	483.7	96.3	0.53	
	QMLS 3	644.0	77.6	0.67	
	QMLS 4	683.3	27.5	0.71	

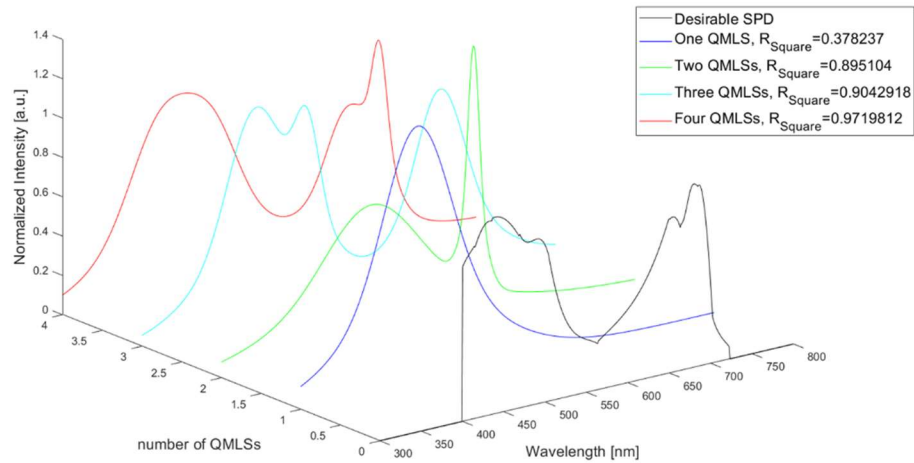


*Fig. 3.10 SPD results using different quantities of ideal QMLSs to fit the photosynthesis action spectrum using ideal QMLSs.*

Table 3.18 and Figure 3.10 show that using more than two QMLSs produces a good fitting performance. The improvement of using four QMLSs instead of three is significant for the PAS applications. Additionally, the simulated results show that an ideal lamp for the PAS application should be built using a combination of CL QMLSs and LEDs to produce a good fit.

# Conclusions and Future work

This work contributes to the design of light sources with specific Spectral Power Distribution profiles to tailor light to the needs of targeted applications. A novel model that combines multiple QMLS to obtain a desired SPD was designed and implemented. The optimization model included the use of genetic algorithms and optimizes not only for the excitation parameters but also models different SPD characteristics for ideal QMLSs.

The dissertation targets emulating three different SPDs obtained from the literature in the fields of preserving museum artifacts and plant growth. The model used LED and CL technologies as artificial light sources. A vacuum testing system was implemented to obtain the SPD profiles of different CL phosphor materials.

To summarize, the GA model works effectively and the most important of its achievements are mentioned below.

- The GA model successfully used the R-square metric to evaluate how much a fitted spectrum emulates the desired spectrum. However, the GA model can also use other methods to evaluate topics such as the CRI and CQS, other color indexes, costs, etc.
- The GA model successfully optimized different fitting coefficients to generate the desired SPDs. Real QMLS and the Ideal QMLS were considered for these GA models.
- The GA model was fast obtaining the fitting coefficients, showing good results even before 50 iterations.



- The experiments show that the GA model with the Real QMLS was successful to validate the accuracy of the theoretical simulations, with an R-Square of 0.97 between the simulated SPD and the experimental SPD.

The analysis section was divided into three. In the first, the GA model successfully optimized fitting coefficients for Real QMLS. In general, the R-square results show a low fitting performance since the emulation can-not modify the peaks and the spectrum widths of the real QMLSs.

In the preserving museum artifacts application, the R-square results for the real QMLS were between 0.1 and 0.015. The low values are due to the mismatch between the peaks positions in the SPDs of the selected QMLSs and the desired SPD: and to the narrow widths of the spectral components of the desired SPD.

In the case of the plant growth's McCree SPD, the best R-square obtained was 0.26 for a group of four LEDs, and the minimum value was 0.156 for a group of two LEDs. It is concluded that the CL QMLSs can offer a better fit using the same number of QMLS, due to their broader FWHM ranges.

In the PAS, the fitted spectrum results show that the best R-Square value is acquired with four LEDs with a value of 0.177 and the worst with 0.055. The results concluded that the spectral width of the desired SPD is a critical requirement. CL QMLSs produce better performances for the PAS targets since they have wider FWHMs ranges than the LEDs. The Red LED does not improve the lamp's overall performance since its peak is both narrow and out of the desirable SPD range.

In the second analysis, the simulated results obtained for the real QMLSs were implemented using the LEDs. The experimental SPDs were measured and evaluated with the R-square. The results confirmed the match between the simulated SPDs and the measured SPDs with an R-square score of at least

In the third analysis, the GA model optimized the fitting coefficients of the peak wavelength, the spectral width, and the peak power using ideal QMLSs based on the blackbody radiation equation. The analysis was performed to create artificial lamps that are composed of one, two, three, and four ideal QMLSs.

In the case of preserving museum artifacts spectrum, the R-square score is significantly higher using three or four QMLSs. The narrow FWHMs values of the QMLSs in the optimization results implied that such a lamp should be constructed using the LED technology. The addition of another QMLS after three QMLSs is not significant enough considering the increment in the total cost with the addition of a new voltage source.

In the case of the McCree SPD, the results show a good fitting performance by using more than two QMLSs. However, the improvement may not be significant when considering additional QMLSs. The results also show that when using three QMLSs, the CL QMLSs can produce a better fit than the LEDs, due to the wider CL spectral width parameters.

In the case of the PAS, the results show that using more than two QMLSs resulted in a good fitting performance. The improvement in using four QMLSs instead of three is significant for the PAS. Additionally, the results show that a PAS-mimicking lamp should be built using a combination of the CL QMLSs and the LEDs to produce a better fit.

In the Future, other variables or fitting coefficients could be added, such as temperature, costs, damage, aging, and energy efficiency. Other fitness functions such as color quality indexes; CRI, CQT, and CCT can be tested. Also, other emulating equations such as the energy created by the light source can be considered. The high speed of the GA optimization approach makes this method useful for application in light engines besides other application such as the IoT, since it could work in real time.

## References

- (1).-R. Haitz, J. Tsao, "Solid-state lighting: 'The case' 10 years after and future prospects" *Physica Status Solidi a applications and science*, [Online] Sep. 2010, vol. 208, no. 1, p. 17–29. Available: <https://doi.org/10.1002/pssa.201026349> [Accessed Dec. 13, 2021]
- (2).- M. Delgado, C. Dirk, J. Druzik, N. WestFall, "Lighting the World's Treasures: Approaches to Safer Museum Lighting", *Color Research and Application*, 2010, vol. 36, no. 4, p. 238-254. [Online] Available: <https://doi.org/10.1002/col.20656> [Accessed Dec. 13, 2021]
- (3).- R. Dang, N. Wang, G. Liu, Y. Yuan, J. Liu, H. Tan, "Illumination in Museums: Four-Primary White LEDs to Optimize the Protective Effect and Color Quality", *IEEE Photonics Journal*, 2019, vol. 11, no. 1 [Online] Available: [DOI: 10.1109/JPHOT.2019.2893822](https://doi.org/10.1109/JPHOT.2019.2893822). [Accessed Dec. 13, 2021]
- (4).- L. Bachouch, P. Dupuis, N. Sewraj, L. Canale, G. Zissis, L. Bouslimi, L. Amraoui, "Tunable multiple-LEDs combination spectrum for plants based on McCree PAR spectrum" *2020 IEEE International Conference on Environment and Electrical Engineering and 2020 IEEE Industrial and Commercial Power Systems Europe (EEEIC / I&CPS Europe)*, 2020, p. 1-6, [Online] Available: [DOI: 10.1109/EEEIC/ICPSEurope49358.2020.9160753](https://doi.org/10.1109/EEEIC/ICPSEurope49358.2020.9160753) [Accessed Dec. 13, 2021]
- (5).- D. Durmus, D. Abdalla, A. Duis, W. Davis, "Spectral Optimization to Minimize Light Absorbed by Artwork", *LEUKOS - Journal of Illuminating Engineering Society of North America*, 2020, vol. 16, no. 1, p.45-54, [Online] Available: <https://doi.org/10.1080/15502724.2018.1533852>. [Accessed Dec. 13, 2021]
- (6).- D. Singh, C. Basu, M. Meinhardt-Wollweber, and B. Roth, "LEDs for Energy Efficient Greenhouse Lighting", *Renewable and Sustainable Energy Reviews*, 2015, vol. 49, p. 139-147, [Online] Available: <https://doi.org/10.1016/j.rser.2015.04.117> [Accessed Dec. 13, 2021]
- (7).- G. Massa, H. Kim, R. Wheeler, A. Cary, C. Mitchell, "Plant Productivity in Response to LED Lighting", *American Society for Horticultural Science*, 2008, vol. 43, no. 7, p. 6, [Online] Available: <https://doi.org/10.21273/HORTSCI.43.7.1951> [Accessed Dec. 13, 2021]
- (8).- J. Jou, C Lin, T. Li, C. Li, S. Peng, F. Yang, J. Thomas, D. Kumar, Y. Chi, B. Hsu, "Plant Growth Absorption Spectrum Mimicking Light Sources" *Materials*, 2015, vol. 8, p. 5265-5275; [Online] Available: [doi: 10.3390/ma8085240](https://doi.org/10.3390/ma8085240) [Accessed Dec. 13, 2021]
- (9).- K. Nikolova, I. Petrinska, D. Ivanov, D. Pavlov, "Investigation of the Photobiological Risk from Blue Light of a Human-Centric Lighting System - Case Study", *2019 11th Electrical Engineering Faculty Conference (BuIEF)*, 2019, p. 1-4. [Online] Available: [DOI: 10.1109/BuIEF48056.2019.9030789](https://doi.org/10.1109/BuIEF48056.2019.9030789) [Accessed Dec. 13, 2021]
- (10).- M. Dong, Y. Sun, J. Qiu and Y. Lin, "Healthy lighting design with low retinal blue light hazard," *2013 10th China International Forum on Solid State Lighting (ChinaSSL)*, 2013, pp. 73-76, [Online] Available: [DOI: 10.1109/SSLCHINA.2013.7177317](https://doi.org/10.1109/SSLCHINA.2013.7177317), [Accessed Dec. 13, 2021]
- (11).- T. Schaeffer, "Effects of Light on Materials in Collections: Data on Photoflash and Related Sources", Getty Publications. [Online]. Available: <https://www.getty.edu/publications/virtuallibrary/0892366451> [Accessed Dec. 14, 2021]

- <sup>(12)</sup>.- D. Durmus, 2018, "Optimizing Light Source Spectrum to Reduce the Energy Absorbed by Objects" Ph.D. Dissertation, The University of Sydney, Sydney, 2017, [Online]. Available: <http://hdl.handle.net/2123/17844>, [Accessed Dec. 13, 2021]
- <sup>(13)</sup>.- E. Zalewski, "Chapter 24: Radiometry and Photometry", Handbook of Optics: Devices, Measurements, and Properties, Volume II, Second Edition, H. Danbury, Danbury, Connecticut, U.S.,
- <sup>(14)</sup>.-R. W. G. Hunt, M. R. Pointer, *Measuring Color*, Published in association with the Society for Imaging Science and Technology. Fourth Edition. 2011.
- <sup>(15)</sup>.-W. Luedtke, J. Livingston, "TECHNICAL MEMORANDUM: IES METHOD FOR EVALUATING LIGHT SOURCE COLOR RENDITION", AN AMERICAN NATIONAL STANDARD, ANSI/IES TM-30-20, 2018, the Illuminating Engineering Society, ISBN# 978-0-87995-379-9 [Online]. Available: <https://www.techstreet.com/standards/ies-tm-30-20> [Accessed Dec. 14, 2021]
- <sup>(16)</sup>.- Davis W., Ohno Y., 2010, "Color quality scale", *Optical Engineering*, 2010, vol. 49, no. 3, [Online] Available: <https://doi.org/10.1117/1.3360335>, [Accessed Dec. 13, 2021]
- <sup>(17)</sup>.- T. Perrin, J. Druzik, N. Miller, *SSL Adoption by Museums: Survey Results, Analysis, and Recommendations*. Office of Energy Efficiency and Renewable Energy, 2015, [Online]. Available: <https://www.energy.gov/eeres> [Accessed Dec. 14, 2021]
- <sup>(18)</sup>.- T. Schaeffer, "Effects of Light on Materials in Collections: Data on Photoflash and Related Sources", Getty Publications. [Online]. Available: <https://www.getty.edu/publications/virtuallibrary/0892366451> [Accessed Dec. 14, 2021]
- <sup>(19)</sup>.- M. Lazzarin, M. Meisenburg, D. Meijer, W. Van Leperen. L. Marcelis, I. Kappers, A. Van der Krol, J. van Loon, M. Dicke, "LEDs Make It Resilient: Effects on Plant Growth and Defense" *Trends in Plant Science*. 2020, vol.26, no. 5, p. 496-508. [Online] Available: <https://doi.org/10.1016/j.tplants.2020.11.013>, [Accessed Dec. 14, 2021]
- <sup>(20)</sup>.- N. Holonyak and S. F. Bevacqua, "Coherent (visible) light emission from Ga (As<sub>1-x</sub>P<sub>x</sub>) junctions", *Applied Physics Letter*, vol. 1, no. 4, p. 82-83, 1962. [Online]. Available: [DOI:10.1063/1.1753706](https://doi.org/10.1063/1.1753706) [Accessed Dec. 15, 2021]
- <sup>(21)</sup>.-Y. Wang, J. M. Alonso and X. Ruan, "A Review of LED Drivers and Related Technologies," in *IEEE Transactions on Industrial Electronics*, vol. 64, no. 7, p. 5754-5765, July 2017, [Online] Available: [doi: 10.1109/TIE.2017.2677335](https://doi.org/10.1109/TIE.2017.2677335), [Accessed Dec. 15, 2021]
- <sup>(22)</sup>.-Z. Yang, M. Gao, W. Wu, X. Yang, X. Wei Sun, J. Zhang, H. Wang, R. Liu, C. Han, H. Yang, W. Li, "Recent advances in quantum dot-based light-emitting devices: Challenges and possible solutions", *Materials Today*, 2019, vol. 24, no. 1369-7021, p. 69-93 [Online]. Available: <https://doi.org/10.1016/j.mattod.2018.09.002> [Accessed Dec. 15, 2021]
- <sup>(23)</sup> E. Jang, S. Jun, H. Jang, J. Lim, B. Kim, Y. Kim, "White-Light-Emitting Diodes with Quantum Dot Color Converter for Display Backlights." *Advanced Materials*. 2010, Vol. 22, no. 28, p. 3076-3080, [Online]. Available: <https://doi.org/10.1002/adma.201000525>, [Accessed Dec. 15, 2021]

- <sup>(24)</sup> E. Schubert, T. Gessmann, J. Kyu Kim, "Light Emitting Diodes", *Kirk-Othmer Encyclopedia of Chemical Technology*, 2005, [Online]. Available: [DOI: 10.1002/0471238961.1209070811091908.A01.PUB2](https://doi.org/10.1002/0471238961.1209070811091908.A01.PUB2) [Accessed Dec. 15, 2021]
- <sup>(25)</sup> J. Wierer, A. David, M. Megens. III-nitride photonic-crystal light-emitting diodes with high extraction efficiency. *Nature Photon* **3**, 2009, p. 163–169 [Online]. Available: <https://doi.org/10.1038/nphoton.2009.21> [Accessed Dec. 17, 2021]
- <sup>(26)</sup> C. Kagan, E. Lifshitz, E. Sargent, D. Talapin, "Building devices from colloidal quantum dots, materials science", *Science*, 2016, vol. 353, no. 6302 [Online]. Available: <https://doi.org/10.1126/science.aac5523> [Accessed Dec. 17, 2021]
- <sup>(27)</sup> H. F. Chinchero and J. M. Alonso, "Review on DC-DC SIMO Converters with Parallel Configuration for LED Lighting Control," *2020 IEEE ANDESCON*, 2020, pp. 1-7, [Online]. Available: [doi: 10.1109/ANDESCON50619.2020.9272083](https://doi.org/10.1109/ANDESCON50619.2020.9272083) [Accessed Dec. 17, 2021]
- <sup>(28)</sup> P. K. Manoilov and A. N. Borodzhieva, "Led Lamps - Money or Health," *2018 IEEE XXVII International Scientific Conference Electronics - ET*, 2018, p 1-4. [Online]. Available: [doi: 10.1109/ET.2018.8549673](https://doi.org/10.1109/ET.2018.8549673), [Accessed Dec. 17, 2021]
- <sup>(29)</sup> A. Jayawardena, D. Duffy and J. Manahan, "Impact of light on safety in industrial environments," *2015 IEEE Petroleum and Chemical Industry Committee Conference (PCIC)*, 2015, p. 1-9, [Online]. Available: [doi: 10.1109/PCICON.2015.7435087](https://doi.org/10.1109/PCICON.2015.7435087) [Accessed Dec. 17, 2021]
- <sup>(30)</sup> S. Kasap, "Principles of Electronic Materials and Devices" *McGraw-Hill*. third edition, 2006.
- <sup>(31)</sup> Cree LED, "XLamp XT-E" LEDs data sheet, CLD DS41 REV 10C [Online]. Available: <https://cree-led.com/media/documents/XLampXTE.pdf> [Accessed Dec. 17, 2021]
- <sup>(32)</sup> Cree LED, "XLamp XP-C" LEDs data sheet, CLD-DS19 REV 13F [Online]. Available: <https://cree-led.com/media/documents/XLampXPC.pdf> [Accessed Dec. 19, 2021]
- <sup>(33)</sup> K. Baran, A. Rózowicz, H. Wachta, and S. Rózowicz, "Modeling of Selected Lighting Parameters of LED Panel", *Energies*, 2020, vol. 13, no. 14. P.467 - 472 [Online]. Available: <https://doi.org/10.3390/en13143583> [Accessed Dec. 19, 2021]
- <sup>(34)</sup> G. Garlick, "The kinetics and efficiency of cathodoluminescence", *British Journal of applied physics*, 2002, vol. 13. [Online]. Available: [DOI:10.1088/0508-3443/13/11/306](https://doi.org/10.1088/0508-3443/13/11/306), [Accessed Dec. 20, 2021]
- <sup>(35)</sup> C. Hunt, A. Chakhovskoi, "Phosphor challenge for field-emission flat-panel displays", *Journal of Vacuum Science & Technology B: Microelectronics and Nanometer Structures Processing, Measurement, and Phenomena*, 1997, vol. 15, p.516 [Online]. Available: <https://doi.org/10.1116/1.589283> [Accessed Dec. 20, 2021]
- <sup>(36)</sup> M. Cao, R. Chacon, C. Hunt, "A Field Emission Light Source Using a Reticulated Vitreous Carbon (RVC) Cathode and Cathodoluminescent Phosphors", *journal of display technology*, 2011, vol. 7, no. 9, [Online]. Available: [10.1109/JDT.2011.2116151](https://doi.org/10.1109/JDT.2011.2116151) [Accessed Dec. 20, 2021]

- <sup>(37)</sup> C. Hunt, S. Blackstone, "High-Quality, Energy-Efficient and Affordable Light Source using Cathodoluminescent Phosphor" [Online]. Available: <https://www.ece.ucdavis.edu/huntgroup/home/publications/> [Accessed Dec. 19, 2021]
- <sup>(38)</sup> T. Hase, T. Kano, E. Nakazawa, H. Yamamoto, "Phosphor Materials for Cathode-Ray Tubes," P. W. Hawkes, *Advances in Electronics and Electron Physics*, Academic Press, 1990, vol. 79, p. 271-373, [Online]. Available: [https://doi.org/10.1016/S0065-2539\(08\)60600-9](https://doi.org/10.1016/S0065-2539(08)60600-9), [Accessed Jan. 2, 2021]
- <sup>(39)</sup> M. Itoh, L. Ozawa, "Cathodoluminescent phosphors", 2006, *Journal of The Royal Society of Chemistry*. Annu. Rep. Prog. Chem. 2006, vol. 102, p. 12-42. [Online]. Available <https://doi.org/10.1039/B417154N>, [Accessed Jan. 2, 2021]
- <sup>(40)</sup> C. Schwarz, L. Chernyak, E. Flitsiyan, "Cathodoluminescence Studies of Electron Injection Effects in Wide-Band-Gap Semiconductors" *Physics Department, University of Central Florida, Orlando, FL, USA*.
- <sup>(41)</sup> L. Wang, X. Wang, K. Takahashi, T. Takashi, N. Hirosaki, R. Xie, "Nitride phosphors as robust emissive materials in white flat field emission lamps", *OPTICAL MATERIALS EXPRESS*, 2017, vol. 7, no. 6, pp. 1934-1941 [Online]. Available: <https://doi.org/10.1364/OME.7.001934>, [Accessed Jan. 2, 2021]
- <sup>(42)</sup> C. Lin, C. Ho, M. Hung, C. Wang, "high voltage driving circuit with negative pulse feature for tubular field emission lamp," 2010, *5th IEEE Conference on Industrial Electronics and Applications*. 2010, p 1118-1123, [Online]. Available: [10.1109/ICIEA.2010.5515846](https://doi.org/10.1109/ICIEA.2010.5515846), [Accessed Jan. 8, 2021]
- <sup>(43)</sup> P. Davari, F. Zare, A. Ghosh and H. Akiyama, "High-Voltage Modular Power Supply Using Parallel and Series Configurations of Flyback Converter for Pulsed Power Applications," in *IEEE Transactions on Plasma Science*, vol. 40, no. 10, p. 2578-2587, Oct. 2012, [Online]. Available: [10.1109/TPS.2012.2199999](https://doi.org/10.1109/TPS.2012.2199999), [Accessed Jan. 8, 2021]
- <sup>(44)</sup> X. He, C. Zhao, Q. He, Y. Gao, Y. Liu, S. Ma, C. Wang, L. Yu, "Simulation of plant growth spectrum with high-fitness based on spectral segmentation fitting". *Optik*, 2021, vol. 230, no. 0030-4026, [Online]. Available: <https://doi.org/10.1016/j.ijleo.2021.166331>, [Accessed Jan. 8, 2021]
- <sup>(45)</sup> O. Ramos, M. Quiroz, E. Mezura, R. Kharel, "Variation Operators for Grouping Genetic Algorithms: A Review", *Swarm and Evolutionary Computation*, 2021, vol. 60. [Online]. Available: <https://doi.org/10.1016/j.swevo.2020.100796>, [Accessed Jan. 8, 2021]
- <sup>(46)</sup> A. Lambora, K. Gupta and K. Chopra, "Genetic Algorithm- A Literature Review," *2019 International Conference on Machine Learning, Big Data, Cloud and Parallel Computing (COMITCon)*, 2019, p. 380-384, [Online]. Available: [10.1109/COMITCon.2019.8862255](https://doi.org/10.1109/COMITCon.2019.8862255) [Accessed Jan. 8, 2021]

# Appendix

This section presents the routines and the main ideas of MATLAB APP implemented in this dissertation. The routines include Color Mixing, R\_Square analysis, and the Genetic Algorithm (GA) discussed in the previous chapters. This section starts with the basics of GA routines to show the iteration process and GA operators; then it explains how they work on optimizing the SPD parameters of QMLS to mimic the target spectrum.

The diagram of a GA routine is shown in Figure A1. The GA begins with an initial population, at this point, all the information is preprocessed and stored in the genes or single elements of the matrix.

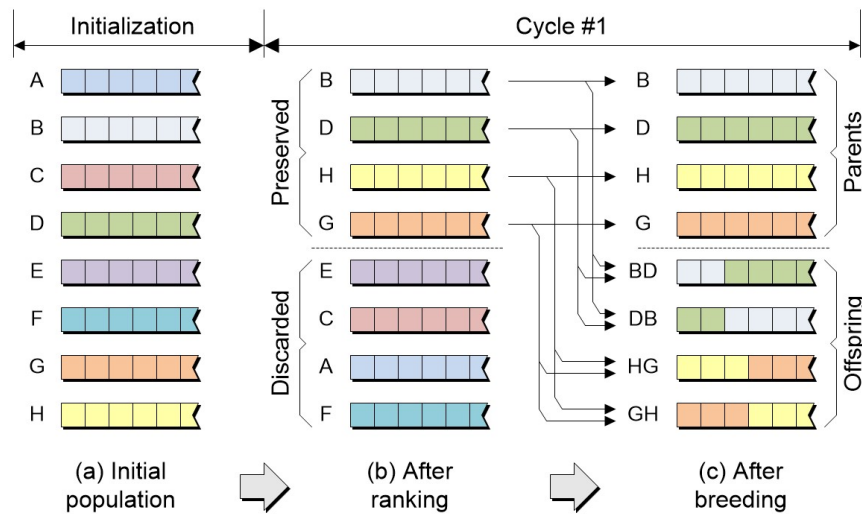


Figure A1: General GA iteration diagram.

After each iteration shown as a cycle in Figure A1, the matrix obtained is called a new generation. The GA will iterate a couple of steps that seek to conserve the information of good chromosomes. The iteration uses the following operators to evolve into the best chromosomes.

- Selection
- Crossover
- Mutation.



## Population and matrix representation

The information of the QMLS is represented in the genes. For example, the current density modifies the light intensity in the LEDs. Then, each column in the Matrix will represent a color light source, and each row produces a final spectrum by combining the color light sources setting. The values are the percentages of the maximum light intensity; a 0 means no light, and a value of 100 means maximum light intensity in this QMLS. Figure A2 shows a row (example) of four columns: QMLS sources of blue, green, yellow, and red light with values of 75%, 25%, 100%, and 50%. All of them are combined to produce a final Spectrum.

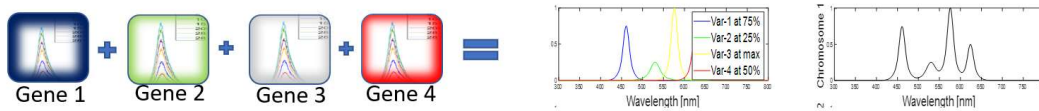


Figure A2. GA diagram for QMLS spectrum generation

## The Ideal QMLS computational representation

The ideal QMLS uses the Black Body Radiation equation (see equation 19, page 50). The equation represented by three variables: peak power, wavelength width or FWHM, and the center or peak wavelength of the QMLS. The code is given in Script 1, and the is presented in Figure A3.

```
i=200:0.5:800;  
Peak=400;  
PeakPower=1;  
SpectralW=110;  
SpectraInt=PeakPower*(exp(-1.*((i-Peak)./SpectralW).^2)+2.*(exp(-1.*((i- Peak)./SpectralW).^2).^5))./3;
```

Script 1: A sample code for an ideal QMLS

In this code, the Black Body Radiation equation will produce an ideal Quasi-Monochromatic Spectrum using the three variables. The wavelength range is given by the variable “i”.

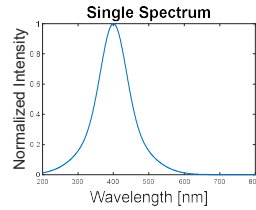


Figure A3: Black Body Radiation spectrum.

### Initial population

The initial population for an ideal QMLS has three variables, each of which will produce a column. The values of each column will be restricted as follow. The columns that refer to the light intensity are normalized, then the values are restricted to floating points between 0 and 1. The value of 0 represents the source without light emission. A value of 1 means the maximum light emission intensity from a single QMLS. The bounds for the spectral width are between 10 nm and 150 nm; the maximum of 150 nm can be obtained using a CL QMLS, and the minimum of 10 nm can be obtained using an LED. The bounds for the peak wavelength are 300 nm and 800 nm. As an example, a 4x12 matrix representing the Initial Population is created by random initialization in Script 2.

```

NumChromosome=4;           % Number of Chromosomes ( fitted curves )
NumGenes=4;                % Number of genes or ((x,y) points)
InitialPopulationIntensity=randi([0 1],NumChromosome,NumGenes); % Initial population for intensity
InitialPopulationWidth=randi([10 100],NumChromosome,NumGenes); % Initial population for spectrum width
InitialPopulationCenter=randi([300 800],NumChromosome,NumGenes); % Initial population for the peak
InitialPopulation=[ InitialPopulationIntensity InitialPopulationWidth InitialPopulationCenter]; % Concatenation

```

Script 2: Random initialization of an Initial Population

Another example is a population in which the light intensity is the only variable that can be modified. It will produce a matrix of one column for QMLS, as is shown in script 3.

```

NumChromosome=4;           % Number of Chromosomes ( fitted curves )
NumGenes=4;                % Number of genes or ((x,y) points)
InitialPopulation=randi([0 1],NumChromosome,NumGenes); % Inicial population

```

Script 3: Initial Population with only one variable or gene for QMLS.

## Evaluation

This operator will use the R\_square equation as the fitness function to compare how the fitted spectrum fits the target spectrum. In Script 4, the fitness function is implemented.

```
function FitnessFunction=R_Square(CurrentGeneration,2);
SSE=sum((Target(x)'-fittedSpectrum).^2);
SST=sum((fittedSpectrum-mean(fittedSpectrum)).^2);
R_Square=SSE/SST
end
```

*Script 4: Fitness function.*

## Selection

The selection operator will preserve the rows that fit better the target spectrum and discard the rows that produce a worse match. The selection ranks and sort the values obtained by the fitness function; then, the better R\_Square get in the top of the matrix and the 50% of the rows are preserved as shown in Script 5.

```
NumPreserved=round(NumChromosome/2); % Number of parents preserved
ParentPreserved=Parent([Rank(1:NumPreserved)],:); % Parents preserved
```

*Script 5: Selection of QMLS.*

## CrossOver

The crossover will create the offspring for the next generation. The offspring created will replace the row positions of the discarded rows (worst values of R\_square). Script 6 shows a crossover example for the QMLS.

```
CrossOverPoint=NumGenes/2; % CrossOver
NumOffspring=round(NumChromosome/2);
Offspring=[ParentPreserved(end,[1:CrossOverPoint])
ParentPreserved(1,[CrossOverPoint+1:end])]; % First Offspring

for i=1:NumOffspring-1;
Offspring(i+1,:)= [ParentPreserved(i,[1:CrossOverPoint])
ParentPreserved(i+1,[CrossOverPoint+1:end])]; % Offspring from 2 to the end
End

CurrentGeneration=[ParentPreserved ;OffspringMutated] ; % New Generation
```

*Script 6: Crossover for QMLS offspring.*

### *Mutation*

The mutation process will introduce random floating values between 0 and 1 into the offspring of the generation. It will increase the variability of the generations avoiding a set of values that lead a local minimum.

```
[rowOffs colOffs]=size(Offspring);  
elemInserted=randi([0 10],1,rowOffs)*0.1;  
PositionMutated=randi([1 rowOffs*colOffs],1,rowOffs);  
Offspring(PositionMutated)=elemInserted;  
OffspringMutated=Offspring;
```

*Script 7: Mutation process.*

### *Stopping Criteria*

The stopping criteria will break or stop the iteration process. Some options for stopping criteria are a maximum number of generations, specific time limits, and error or tolerance values.

In this dissertation, the GA is implemented with a Matlab ToolBox. The function name is *ga*, and it is shown in Script 8. In the script, the function *fun* contains the *Fitness function, color mixing, and the QMLS information data*. The *lb* and *ub* are the bounds of the genes. The *N\_QMLS* is the number of QMLS used to construct the final spectrum.

*Optimoptions* are used to set the GA operators. In the script, the stopping criteria are set with a *MaxGeneration*, which uses a maximum number of generations to stop the algorithm. A graph that informs the current generation's performance could be set with *PlotFcn*. In this case, it is set to show the best and mean fitness values of each generation. This can be seen in Figure A4.

```
fun=@R2Eval;  
  
lb = ones(N_QM,1)*(0.0);  
ub = ones(N_QM,1)*4;  
  
options = optimoptions('ga','PlotFcn', @gaplotbestf);  
%opts = optimoptions(opts,'MaxGenerations',300,'MaxStallGenerations', 100);  
  
[peakP,fval,output] = ga(fun,N_QMLS,[],[],[],[],lb,ub,[],options) ;
```

*Script 8: GA implementation for ideal QMLS*

The ga call's function argument named fun is shown in Script 9. It contains the Fitness Function, the color mixing, and the gene and chromosome implementation.

The routine is implemented by loading a matrix that has the fitted spectra in each row. The second load command is for a 1D array which has the target spectrum's information as shown in Section 1 of Script 9. Section 2 has a filter that eliminates the range in which the comparison is not applicable. It increases the accuracy of the R\_Square metric. Section 3 introduces the gene modification for each color. This section also predicts the fitted curve by using color mixing. Section 4 shows how the R\_Square can be applied to compare the two spectra.

```
function R2=R2Eval(peakP)

% Section 1 - Loading
load 'QMSelected.mat' % Quasi-Monochromatic light sources selected
load('TargetSelected.mat'); % target Selected
[c N_QM]=size(QMSelected); % size the matrix of Spectra
NewTarget=TargetSelected;% aux variable

% Section 2 - filter
[x y]=find(NewTarget>=0.001);
peakP=[0.1000 1.72 0.64] % Chromosome
N=1:length(y);
NewSPD=0;

% Section 3 – Gene modification and Color mixing
for a=1:N_QM

    NewSPD=peakP(a).*QMSelected(:,a)+NewSPD; % gene modification and color mixing

end

% Section 4 – Fitness funtion
NewSPDA=NewSPD(x); % Aux Variable
ybar=mean(NewSPDA);

% R_Square Analysis
SSE=sum((NewTarget(x)'-NewSPDA).^2);
SST=sum((NewSPDA-ybar).^2);
R2=SSE/SST
% plot(300:800,NewSPD,300:800,NewTarget) % plot available
end
```

*Script 9: Fitness function calculation routine.*

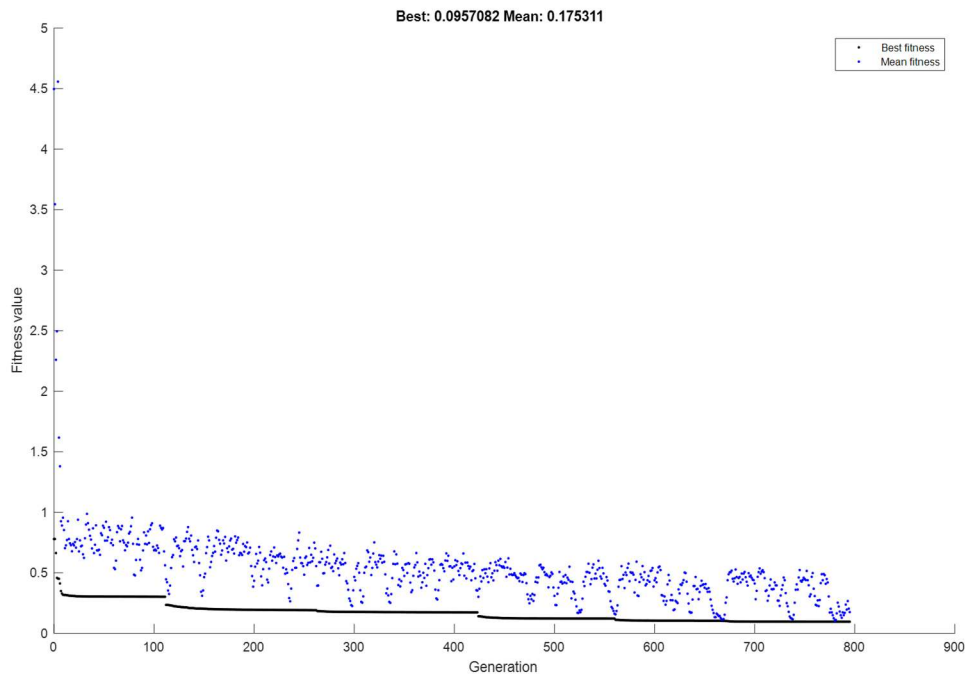


*Figure A4: Plot of the best and mean fitness values as a function of the number of iterations.*

In Script 8, the function PlotFcn was called. It specifies the plot function or functions called at each iteration by ga. The PlotFcn option was set to be a built-in plot function. The algorithm can be stopped anytime by clicking the **Stop** button on the plot window.